12-2017

Remediation of Trivalent and Hexavalent Chromium Ions from Aqueous Solutions Using Titanium Dioxide Polymorphs

Yvette Cantu
The University of Texas Rio Grande Valley

REMEDIATION OF TRIVALENT AND HEXAVALENT CHROMIUM IONS FROM AQUEOUS SOLUTIONS USING TITANIUM DIOXIDE POLYMORPHS

A Thesis

by

YVETTE CANTU

Submitted to the Graduate College of
The University of Texas Rio Grande Valley
In partial fulfillment of the requirements for the degree of

MASTER OF SCIENCE

December 2017

Major Subject: Chemistry

REMEDIATION OF TRIVALENT AND HEXAVALENT CHROMIUM IONS FROM AQUEOUS SOLUTIONS USING TITANIUM DIOXIDE POLYMORPHS

A Thesis
by
YVETTE CANTU

COMMITTEE MEMBERS

Dr. Jason G. Parsons
Chair of Committee

Dr. Evangelia Kotsikorou
Committee Member

Dr. Jose J. Gutierrez
Committee Member

Dr. Frank Dean
Committee Member

December 2017

ABSTRACT

Cantu, Yvette, Remediation of Trivalent and Hexavalent Chromium Ions from Aqueous Solutions using Titanium Dioxide Polymorphs. Master of Science (MS), December, 2017, 56 pp., 11 tables, 23 figures, references, 20 titles.

Three titanium dioxide (TiO_2) polymorphs were synthesized and used for the removal of chromium (III) and chromium (VI) from aqueous solutions. Various solution parameters were studied to determine the effects of pH, temperature, time, possible interfering ions, and capacities on the binding of Cr(III) and Cr(VI) to all three polymorphs. pH assays determined the optimum pH for the binding of both Cr(III) and Cr(VI) to each polymorph. Adsorption isotherms determined that the adsorption of Cr(III) was non-spontaneous for the three polymorphs with ΔG values ranging from 6.03 to 12.89 kJ/mol. Furthermore, the binding of Cr(VI) to anatase was also non-spontaneous with values ranging from 1.81 to 10.72 kJ/mol. The binding of Cr(VI) for both brookite and rutile was spontaneous with ΔG values ranging from -0.22 to -3.04 kJ/mol.

DEDICATION

I would like to dedicate this work to my family. My mom and dad for always believing in me, and encouraging me to continue and finish my studies. My little brother, Victor Cantu for taking the time to help me out when the loads got big. And above all, my brother Jesus Cantu for always sticking by my side and going above and beyond to ensure my completion of this work. Without his ongoing guidance, patience, and dedication none of this would have been possible.

ACKNOWLEDGMENTS

I would like to express my deepest gratitude to my advisor, Dr. Jason G. Parsons, for his unconditional help. I would especially like to thank him for giving me the opportunity to work in his lab, as well as for guiding me throughout my coursework. Without his knowledge, patience and guidance this work wouldn't have been possible.

I would like to thank my committee members: Dr. Evangelia Kotsikorou, Dr. Frank Dean, and Dr. Jose J. Gutierrez for their knowledge and expertise as well as their willingness to assist me in this work.

I would like to thank former students Carlos Tamez and Juan Leal for giving me the foundation needed in order to accomplish my work, as well as Maria Dolores Pacheco for all her guidance and expertise. Above all, I would like to thank my brother Jesus Cantu for always lending a hand and pushing me to finish and graduate. Without his determination and ongoing guidance this work wouldn't have been accomplished. I would also like to thank Carolina Valdes, Kenneth Flores, and Diego F. Gonzalez for all their guidance and assistance in lab.

TABLE OF CONTENTS

Page

LIST OF TABLES

Page

LIST OF FIGURES

Page

CHAPTER I

INTRODUCTION

Contamination of Water by Heavy Metals

Water is an essential component for all living things, and as such, sufficient amounts are needed on a daily basis. However, approximately 2% of all the water found on Earth can be considered freshwater. The continual industrialization of the world has affected the accessibility to potable water has become a significant global concern. Since industrialization of the world, contamination of fresh water has increased significantly from organic and inorganic chemical pollutants. Organic pollutants are chemicals that are mostly composed of carbon and hydrogen atoms [1]. Additionally, organic compounds can contain other elements such as oxygen, nitrogen, sulfur, phosphorus, and chlorine, which are commonly known as hetro-atoms [1]. Presently, there are over 70,000 chemicals commercially used of which the United States Environmental Protection Agency (EPA) has identified 654 as hazardous [1]. Many of these hazardous chemicals include pesticides, herbicides, fertilizers, degreasers, petroleum components, and industrial manufacturing by-products. Inorganic pollutants are chemicals that do not contain carbon. Furthermore, these compounds are non-biodegradable and persistent pollutants in the environment.

Inorganic pollutants include compounds such as mineral acids, inorganic salts, trace elements, metal ions, organometallic compounds, and metal compounds [2]. Significant amounts of heavy metal contaminants in the environment arise from natural sources as well as release by

different anthropogenic activities. Anthropogenic that release heavy metals into the environment include processes such as: surface finishing, paint and pigment production, battery manufacturing, the mining and smelting of ores, oil refining, leather tanning, electroplating, and among others [3]. Examples of heavy metals commonly found in water and sewage systems include the following: lead, mercury, chromium, nickel, cadmium, selenium, uranium, zinc, and arsenic [3]. These heavy metals are highly toxic and poses significant health risks after prolonged periods of exposure. Some of the health risks associated with these heavy metals include damage to the following vital organs and body systems: bones, liver, lungs, kidneys, endocrine glands, gastrointestinal system, cardiovascular system and the central nervous system [4]. In addition, prolonged exposure to heavy metals has been linked to various degenerative diseases as well as increased risks for cancer.

Chromium is a transition metal that is naturally present in the environment. Chromium is ubiquitous and is found in the biotic and abiotic parts of the environment. Furthermore, chromium is tasteless and odorless [6]. Chromium has many oxidation states, however, the two most common oxidation states in wastewaters and the environment are trivalent chromium (Cr III) and hexavalent chromium (Cr VI). Both of which have very different and have distinctive properties. For example, chromium(III) is an essential dietary supplement found in fruits, vegetables, meats, grains, and yeast. The primary function of chromium(III) in the human body is to help metabolize fats and carbohydrates and break down insulin. In addition, chromium(III) aids in the synthesis of fatty acids and cholesterol [6]. On the other hand, chromium(VI) is highly toxic. Chromium(VI)has the ability to become a carcinogenic agent through modifications of the DNA transcription process leading to chromosomic aberrations [3]. According to the USEPA it was reported that approximately 97,379 pounds of chromium get released annually into the

environment [7]. The majority of the chromium released comes directly or indirectly from industrial activities, which include but are not limited to inadequate storage, inadequate disposal methods, leakages, nuclear power plants, textile industries, paints production, leather processing, electroplating, and steel production [3,4].

The USEPA is a well-known organization for setting appropriate contaminant standards for drinking water. The Safe Drinking Water Act (SDWA) requires the EPA to establish regulations on the total level of contaminants so that no adverse health effects will occur upon exposure. The contaminant standards are often set at maximum contaminant levels (MCL). An MCL is the maximum allowed level of a specific contaminant in water that should not have detrimental effects on people. The MCL standards are set to maintain health goals after considering the cost of remediation, benefits and the ability to remove contaminants with the adequate technology needed. The EPA standard for chromium was established in 1991 and set to 0.1 milligrams per liter (mg/L) [5]. This MCL has been set for total chromium in the water, which includes both chromium (III) and chromium (VI) in potable waters.

Current Methods for Heavy Metal Remediation

Currently, there is are a wide variety of methods, which are applicable to the remediation of chromium from contaminated wastewaters. Conventional or traditional methods include chemical precipitation, membrane filtration, electrodialysis and reverse osmosis. However, most of the afore mentioned methods have major problems with their usage. For example, chemical precipitation although a simple process where the precipitation of metals is achieved by adding a coagulant, such as iron salts, lime, alum or an organic polymer, to the water has a number of drawbacks. Although coagulation/precipitation is cost effective it produces large amounts of

waste in the form of sludge that has to be disposed, which increases the overall operating costs of the process. Membrane filtration is a purification technique requiring a pressure driven system to force the contaminated water to permeate through a membrane, producing purified water. The primary mechanisms in this process are a combination of size exclusion, surface chemistry, and electrical charge [4]. The main advantage of membrane technology is that it requires a relatively small operation space. However, the disadvantages of membrane technology include the high costs of the membranes, which are fragile, generally easy to clog, as well as high pressure pumping systems. In general membrane technologies and reverse osmosis water treatment systems have extremely high operational costs. Electrodialysis is a separation technique that uses a semi-permeable membrane with an electric potential. The membranes are either cation or anion exclusive, which means that membranes will either allow positive or negative matter flow through depending on the charge applied to the membrane [4]. Although electrodialysis is a highly selective technique the operational cost is extremely high due to the massive energy consumption of the process.

Researchers have developed much more cost-effective methods to treat both potable and industrial wastewater containing toxic metal ions. Adsorption, is a passive technique that is both cost effective and simple to employ. It utilizes materials, or sorbent, that adsorb the contaminants in from the waste. Newer technologies have been investigating nanomaterials as the adsorbents, which have been shown to be efficient and economical in the removal of heavy metals from water. The high efficiency of nano-adsorption has been due to the properties of nanomaterials, which include a large surface area: volume ratio and highly reactive surfaces, which enables them to remove larger amounts of metal ions [7,8]. In addition, some nanomaterials exhibit magnetic properties that enables them to be removed by magnetic

separation once the remediation process is complete [4,7]. One of the main properties of nanomaterials is that it makes the process cleaner and more efficient. Examples of low cost adsorbents utilized for the removal of metal ions include: metal oxides, graphene oxide, carbon nanotubes, zeolites, clay, chitosan and chitin, pomegranate peel, sawdust, activated carbon, cotton, and various types of tree bark [4,7,8,9].

Proposed Nanomaterial Adsorbents

Titanium dioxide has obtained attention due to its many properties and different polymorphs. In the present study, the three polymorphs of TiO_2 were synthesized and investigated for the removal of chromium (III) and chromium (VI) in contaminated water. The three polymorphs of TiO_2 include: anatase, brookite, and rutile, all of which have slightly different crystal lattices, different photocatalytic properties, surface structures, as well as chemical properties. The rutile polymorph was synthesized via hydrothermal reaction, the anatase and brookite polymorphs were synthesized using a reflux method. Batch studies were developed to investigate effects of pH, temperature, time, possible interfering ions, and binding capacities of all three polymorphs. In addition, the thermodynamic properties of chromium(III) and chromium(VI) binding to the three polymorphs of TiO_2 were investigated.

CHAPTER II

MATERIALS AND METHODS

Synthesis of Titanium Dioxide Nanomaterial

Synthesis of Anatase Nanomaterial

The synthesis of the anatase polymorph was achieved through the following process: 223 mL of a 0.166 M solution of sodium sulfate (Na_2SO_4) was prepared with ultra-pure water (18Ω H_2O) and added to a 500-mL round bottom flask. Then 27 mL of a 20 % $TiCl_3$ in 2N HCl was added to the Na_2SO4 solution. The concentration of both the reagents Na_2SO_4 and $TiCl_3$ were equivalent to each other in the final solution at 0.166 M. Then O_2 flow was into the solution at a rate of 100 mL/min and the reaction was refluxed at 100˚C for 8 h. Subsequent to reaction, the product was centrifuged at 3800 rpm for 10 min and the supernatant was decanted. The white precipitate was then washed twice using ultra-pure water with centrifugation the supernatants were discarded. Finally, the white precipitate was dried at 45˚C overnight and prepared for characterization.

Synthesis of Brookite Nanomaterial

The synthesis of the brookite polymorph was performed in a similar fashion to the anatase polymorph. A 0.166 M sodium acetate was prepared with 223 mL ultra-pure water and added to a 500-mL round bottom flask and 27 mL of $TiCl_3$ in 2N HCl was added to the sodium acetate solution. The concentration of both the reagents sodium acetate and $TiCl_3$ were equivalent to each other in the final solution at 0.166 M. Then O_2 was introduced into the

reaction mixture a rate of 100 mL/min and kept constant throughout the reaction. The mixture was then refluxed at 100˚C for 8 h. After reaction, the product was centrifuged at 3500 rpm for 10 min and the supernatant was decanted. The precipitate was then washed with twice with ultra-pure water and centrifuge between washing. All supernatants were discarded subsequent to washing cycle. The precipitate was then oven-dried at 45˚C overnight and prepared for characterizations.

Synthesis of Rutile Nanomaterial

The rutile polymorph synthesis was achieved through a hydrothermal reaction method. In the synthesis, $TiCl_4$ was added to ultra-pure water at a 1:30 ratio under stirring. A total of 50 mL of $TiCl_4$ was added to 250 mL of ultra-pure water, which was previously cooled to 1.0˚C prior to addition. The addition was performed using an addition funnel and constant stirring. After addition of $TiCl_4$, the mixture was transferred into Teflon lined autoclaves which were filled to approximately 80% of their capacity. The autoclaves were sealed and placed in an oven at 110˚C for 3 hours of reaction. The autoclaves were then cooled naturally to room temperature and opened. The samples were then centrifuged at 3500 rpm for 10 min and the supernatant was decanted. The precipitate was then washed twice with ultra-pure water and centrifuged between each washing cycle. The precipitate was then oven-dried at 45˚C overnight and prepared for characterizations.

X-ray Diffraction Analysis (XRD)

The XRD characterization was performed using a Rigaku Miniflex diffractometer with a copper source (kα=1.54 Å), a nickel filter, step width 0.05˚, a counting time of 5 s, and a scintillation detector. The XRD data was collected from 20˚ to 60˚ in 2θ. Furthermore, the XRD

patterns were compared to literature data for the synthesized material. The XRD patterns were fitted using the LeBail fitting process in the Fullprof software and crystallographic data from the literature [10].

Scanning Electron Microscopy (SEM) Analysis

SEM Micrographs of the samples were obtained using a Zeiss Evo LS scanning electron microscope. The samples were fixed onto stages with a polymer adhesive and sputter coated with palladium to induce conductivity. The process for sputter coating was performed using a Denton vacuum sputter coater for 35 seconds at 45 mV. The voltage and magnification for each sample varied.

RAMAN Spectroscopy

The RAMAN spectra were collected on a Bruker Senterra Raman Microscope. The instrumental collection parameters were as follows: a laser with a wavelength of 785 nm, a 25 μm aperture, a 5s sampling time, and 25 co-additions. The anatase and brookite RAMAN spectra were done using the same conditions. Furthermore, the sample data was also collected at a power of 10 mW with a 4 cm^{-1} resolution.

pH Profile

The effect of pH on the binding of chromium (III) and chromium (VI) were tested on the adsorption onto nanomaterials (anatase, brookite, and rutile) from pH 2 through pH 6. A concentration of 3 parts per million (ppm) was used to determine the optimal binding pH. Initially, the 3ppm solutions were created followed by the pH adjustment of each solution to the

specific pH value. The pH adjustment was performed using either dilute sodium hydroxide or dilute nitric acid. At each desired pH, a 4.0 mL aliquot was removed and transferred to a 5.0 mL test tube, which contained 10 mg of the nanomaterial. The aliquots were extracted in triplicate for statistical purposes. In addition, control samples at each pH were also create, which consisted of the pH adjusted solution in the absence of the nanomaterials. The tubes were then capped and equilibrated on a rocker for one hour. Subsequent to reaction the samples and controls were centrifuged at 3500 RPM for 10 minutes. The supernatants were collected and stored for further analysis using ICP-OES.

Capacity Studies

The binding capacity of the titanium dioxide nanomaterials was determined utilizing batch isotherm studies. The isotherm studies were performed using either chromium(III) or chromium(VI)solutions with concentrations of 0.3, 3, 30, 100, 300, and 1000 ppm. The solutions were pH adjusted to the optimum binding pH and transferred to a 5mL tube that contained 10mg of the nanomaterial. In addition, control samples at each pH were also create, which consisted of the pH adjusted solution in the absence of the nanomaterials. Each concentration was repeated in triplicate for both the samples and the controls for statistical purposes. The tubes were capped and equilibrated on a rocker for one hour. Subsequent to equilibration the samples and controls were centrifuged at 3500 RPM for 10 minutes. The supernatants were decanted and stored for analysis using ICP-OES.

Thermodynamic Studies

Thermodynamic studies were conducted for both the chromium(III) and chromium(VI) ions at the temperatures of 4°C, 21°C, and 45°C. The study was performed in conjunction with the capacity studies. The reactions were performed using chromium(III) ad chromium(VI) solution with the following concentrations: 0.3, 3, 30, 100, 300, and 1000 ppm. The solutions were pH adjusted to each nanomaterial's optimal binding pH and reacted at the desired temperature. For the reactions, 4.0 mL aliquots of each concentration were transferred into tubes containing 10 mg of either anatase, brookite, or rutile nanomaterial. In addition, control samples at each pH were also created, which consisted of the pH adjusted solution in the absence of the nanomaterials. The solutions were equilibrated for 1 hour on a rocker at the specified temperatures. The reaction samples and control tubes were centrifuged at 3500 RPM for 10 min, subsequent to the equilibration. The supernatants were decanted and saved for further analysis.

Kinetic Studies

Studies were conducted at various time intervals and different temperatures in order to determine kinetics and the activation energy of the reaction. The reactions were all performed at the optimum binding pH, as was determined from the pH profile study. The pH of the solutions was adjusted using either dilute nitric acid or dilute sodium hydroxide. Reactions were performed using a concentration of 30ppm of either the chromium(III) or the chromium(VI). 4.0 mL aliquots of the pH adjusted solutions were added to tubes containing 10mg of either anatase, brookite, or rutile nanomaterial for the sample solutions. In addition, control samples at each pH were also create, which consisted of the pH adjusted solution in the absence of the nanomaterials. The samples and controls were sealed and equilibrated at the following

temperatures 4°C, 21°C, and 45°C at for the following time intervals: 5, 10, 15, 30, 60, 90, and 120 minutes. Subsequent to equilibration, the samples were centrifuged at 3500 RPM for 10 minutes, and the supernatants were decanted into clean test tubes and saved for further analysis.

Interference Studies

Studies were performed to determine the interference common cations and anions found in natural water systems that could have an effect on the binding of chromium(III) and chromium(VI) ions onto titanium dioxide polymorphs. The interfering ions were selected based on the ionic charge of the chromium being studied. For chromium(III) the following cations were selected: Ca^{2+}, K^{+}, Mg^{2+}, Na^{+}. Whereas, for chromium(VI) the following anions were selected: Cl^{-}, NO_3^{-}, SO_4^{2-}, and PO_4^{3-}. The solutions were prepared at a concentration of 300 ppb of either chromium(III) or chromium(VI). The interfering ions were added to the chromium(III) or chromium(VI) solutions at the following concentrations: 0.3 ppm, 3 ppm, 30 ppm, 100 ppm, 300 ppm, and 1000 ppm, using individual ionic solutions. In addition, a combined interference solution containing either all the cations or anions were created to investigate the effects of combined interferences on the chromium(III) and chromium(VI) binding. Both the cationic and anionic solutions were pH adjusted to the optimum binding pH. As mentioned earlier, the pH adjustment was performed using either dilute nitric acid or dilute sodium hydroxide. Aliquots of 4.0 mL of the pH adjusted solutions were added to tubes containing 10 mg of either anatase, brookite, or rutile nanomaterial for the sample solutions. In addition, control samples at each pH were also created, which consisted of the pH adjusted solution in the absence of the nanomaterials. The reaction samples and controls were then equilibrated on a rocker for 1 hour.

Subsequent to equilibration, the samples and controls were centrifuged at 3500 RPM for 10 minutes, the supernatants were decanted, and saved for further analysis.

ICP-OES/ GFAAS Analysis Parameters

For the analysis of the batch studies, a Perkin Elmer Optima 8300 (Perkin Elmer, Shelton CT) or PinAAcle 900Z atomic absorption spectrometer (Perkin Elmer, Shelton CT) with Winlab32 software were used. All samples that were analyzed fell within the values for the calibration. If the samples were too concentrated, they were diluted to fit within the limits of the calibration curve. The operation parameters for the ICP-OES and GFAAS analyses are shown in Table 1 and Table 2, respectively. In addition, the chromium(III) and chromium(VI) were analyzed with calibration curves with correlation coefficients (R^2) of 0.99 or better.

Table 1: ICP-OES Parameters for the Analysis of Cr(III) and Cr(VI) Solutions after Reaction with TiO_2 Polymorphs

Parameter	Settings
λ	267.716 nm
RF power	1500 W
Nebulizer	Gemcone (low flow)
Plasma Flow	15 L/min
Auxiliary Flow	0.2 L/min
Nebulizer Flow	0.55 L/min
Sample Flow	1.50 mL/min
Injector	2.9 mm Alumina
Spray Chamber	Cyclonic
Integration Time	20 seconds
Replicates	3

Table 2: GFAAS Parameters for the Analysis of Cr(III) and Cr(VI) Solutions after Reaction with TiO_2 Polymorphs at a λ 357.87 nm.

	Temperature (˚C)	Ramp time (s)	Hold time (s)
Pre-dry	110	1	30
Dry	130	15	30
Char	1500	10	20
Atomization	2300	0	5
Clean out	2450	1	3

CHAPTER III

RESULTS AND DISCUSSION

Nanomaterial Characterizations

Three polymorphs of titanium dioxide were synthesized using hydrothermal processes. The three polymorphs are anatase, brookite, and rutile. The geometry for Anatase is tetragonal (4/m 2/m 2/m) with its space group being I 41/amd—the unit cell parameters are a = 3.7845 Å, c = 9.5143 Å; (Z =4) [10]. Anatase is one of the most used materials in photo-catalysis and photovoltaics. Brookite takes on an orthorhombic dipyramidal (2/m 2/m 2/m) geometry with its space group being PCAB and the unit cell parameters are a = 5.4558 Å, b = 9.1819 Å and c = 5.1429 Å; (Z = 8) [10]. Brookite is the least thermodynamically stable of the three and is the rarest of all three TiO_2 phases. In addition, the methods of synthesis are not very prevalent in the literature, consequently there not much research has been performed into this material's properties. On the other hand, rutile is the most stable of the three TiO_2 phases and is widely used as a pigment and for photo-oxidation of organics with anatase in thin films. Rutile has a body-centered tetragonal unit cell (4/m 2/m 2/m) taking on a space group of P 4/mnm, with the unit cell lattice parameters of a=b=4.584 Å, and c=2.953 Å; (Z=2). Figures 1, 2 and 3 show the structures of anatase, brookite and rutile using polygons, respectively [10]. As can be seen in Figures 1-3 the different phases of TiO_2 have structural differences. Both anatase and rutile are very ordered with repeating units of the polygons. However, brookite has a more disordered

array of the polygons, a higher amount of distortion is visible in the crystal which would explain the lower thermodynamic stability of this phase.

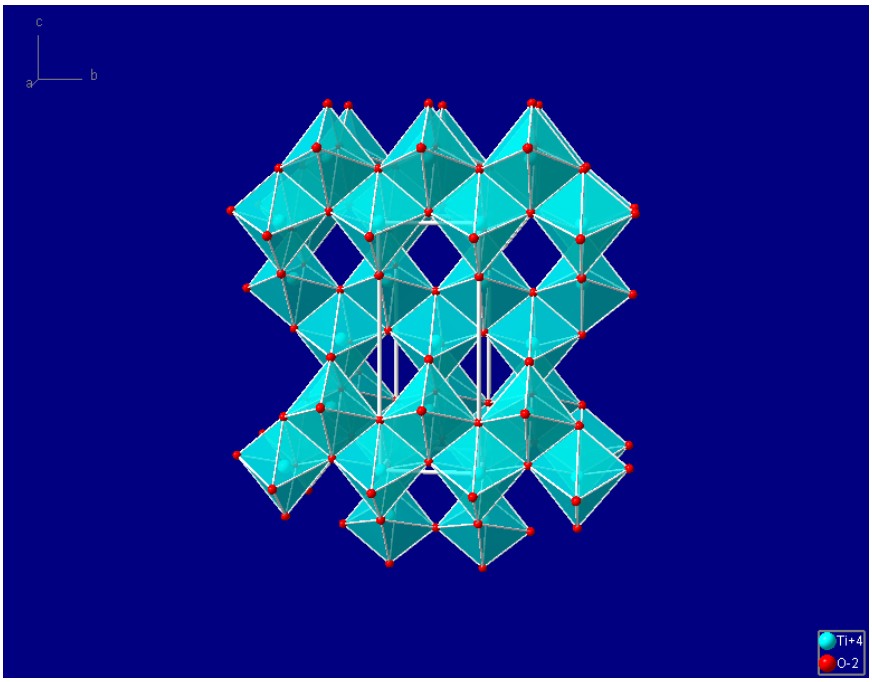

Figure 1: Structure of Anatase from Literature

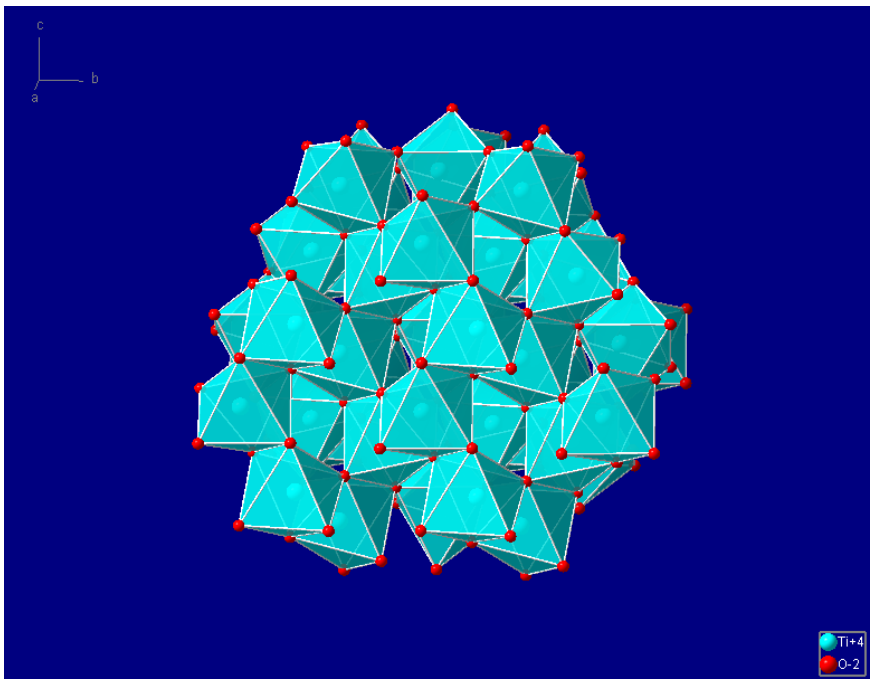

Figure 2: Structure of Brookite from the Literature

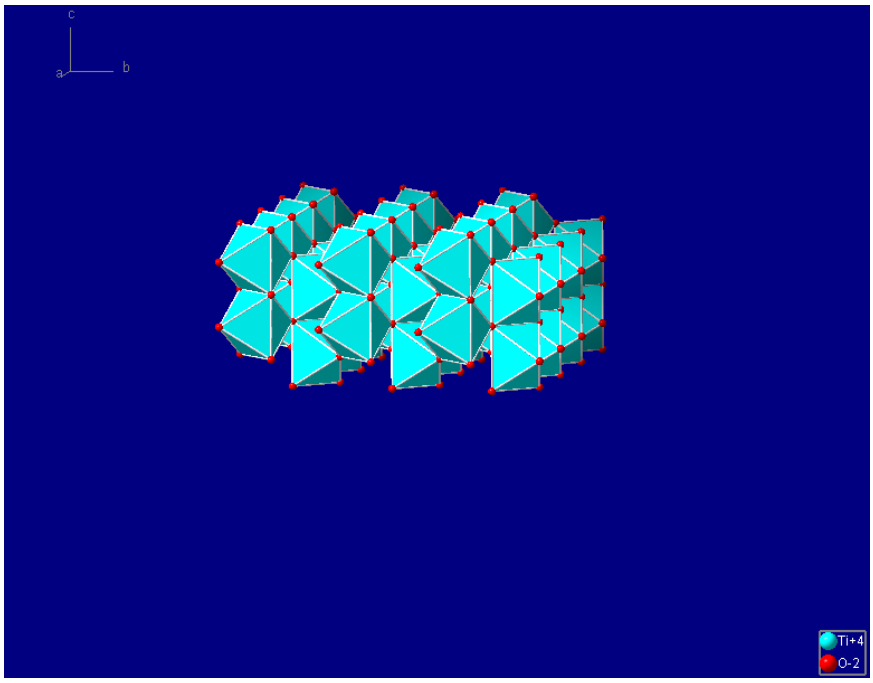

Figure 3: Structure of Rutile taken from the Literature

Table 3: XRD Fitting Data Obtained from the Fullprof Fitting of the Synthesis for Brookite and Anatase from the 100°C Synthesis.

Sample	Cell	a(Å)	b(Å)	c(Å)	χ^2
Rutile	P42/MNM	4.629	4.629	2.951	1.22
Brookite	PBCA	9.201	5.443	5.149	2.06
Anatase	I41/AMDS	3.801	3.801	9.501	1.46

Note: in all the lattices the $\alpha=\beta=\gamma=90$

The diffraction pattern for the collected data from the rutile synthesis is shown in Figure 4. These Bragg peaks correspond to the 110,101, 200, 111, 210, 211, and the 220, planes for rutile phase of TiO_2 with a P42.MNM space group. The Bragg peaks are located at 27.2, 36.1, 38.9, 41.1, 43.7, 54.1, and 56.2˚in 2θ, respectively. In addition, the calculated lattice parameters for the rutile phase are presented in Table 3 which correspond to the literature data [10]. Furthermore, the χ^2 for the fitting was 1.22 indicating a high goodness of fit between the literature crystal structure and the collected diffraction pattern. It should be noted that a χ^2 below 5 in fitting of X-ray diffraction patterns indicates a high goodness of fit between the data and the calculated pattern.

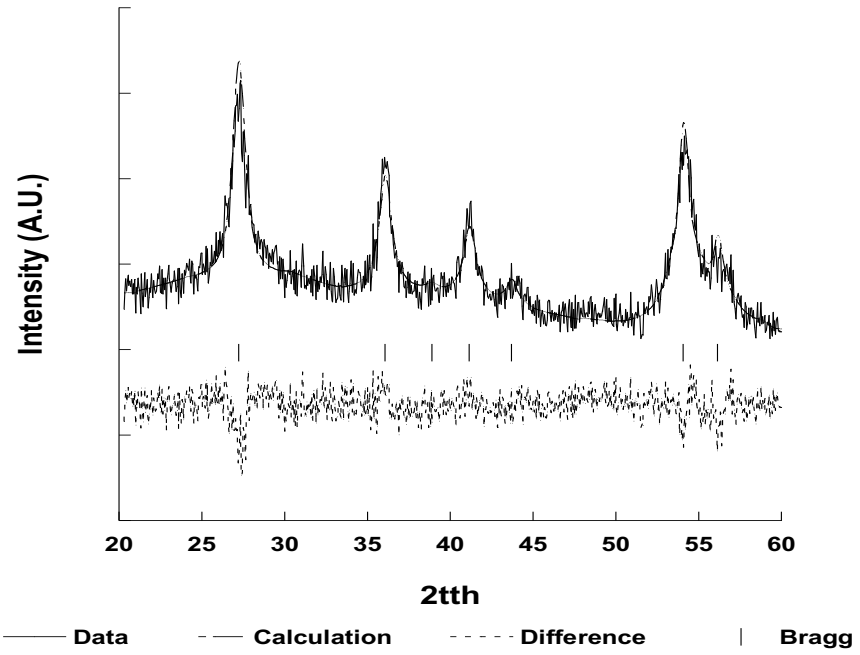

Figure 4: FullProf Fitting of the Rutile Diffraction data obtained at the 110°C Temperature.

Figure 5 shows the diffraction pattern for the collected data from the brookite synthesis and the Fullprof fitting. The Bragg peaks are indicated by the vertical lines in the figure. The Bragg peaks observed in the diffraction correspond to the 111, 210, 211, 020, 102, 021, 311, 220, 121, 202, 221, 212, 302, 022, 312, 122, 222, 131, 113, and the 213 planes of Brookite. The diffraction planes are located at 25.6, 25.8, 30.9, 33.1, 35.4, 37.3, 38.4, 38.6, 38.9, 39.2, 39.6, 42.6, 43.1, 45.8, 48.1, 49.2, 52.5, 54.7, and 55.8 in 2θ. In addition, the brookite was found to crystallize with a space group of PBCA and the lattice parameters shown in Table 3 [10]. Furthermore, the $\chi 2$ for the fitting was 2.06 indicating a high goodness of fit between the literature crystal structure and the collected diffraction pattern.

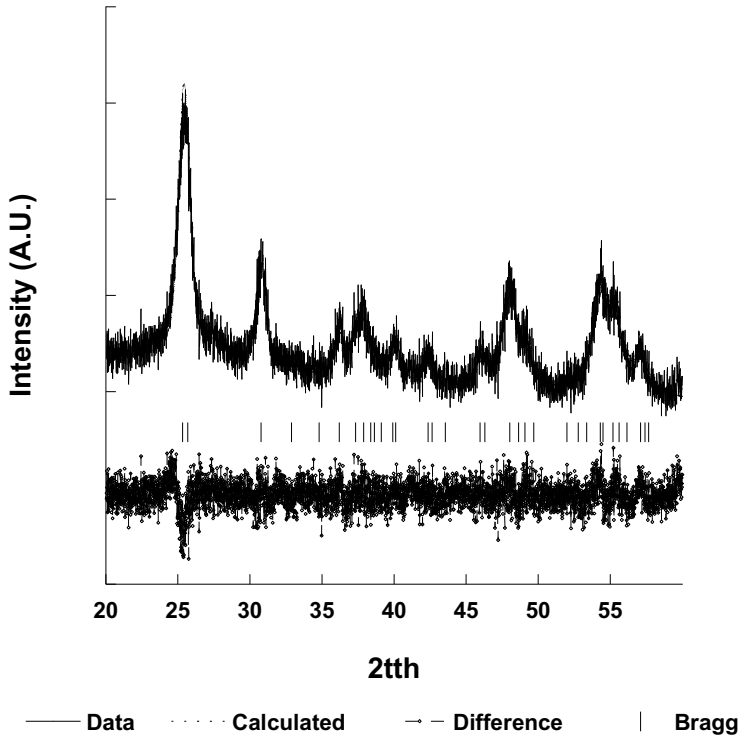

Figure 5: FullProf Fitting of the Brookite Diffraction data obtained at the 100°C 8 hr Reflux sing sodium acetate.

Figure 6 shows the diffraction pattern for the collected data from the anatase synthesis and the Fullprof fitting. The Bragg peaks are indicated by the vertical lines in the figure. The Bragg peaks correspond to the 101, 103, 004, 112, 200, 202, 105, 211 planes of the Anatase phase of TiO_2. The diffraction planes are located at 25.2,36.9,37.8,38.4,47.8,51.7,58.9, and 54.7° in 2θ. In addition, the Anatase was found to crystallize into the I41/AMD space group with lattice parameters presented in Table 3 [10]. Furthermore, the χ^2 for the fitting was 1.46 indicating a high goodness of fit between the literature crystal structure and the collected diffraction pattern.

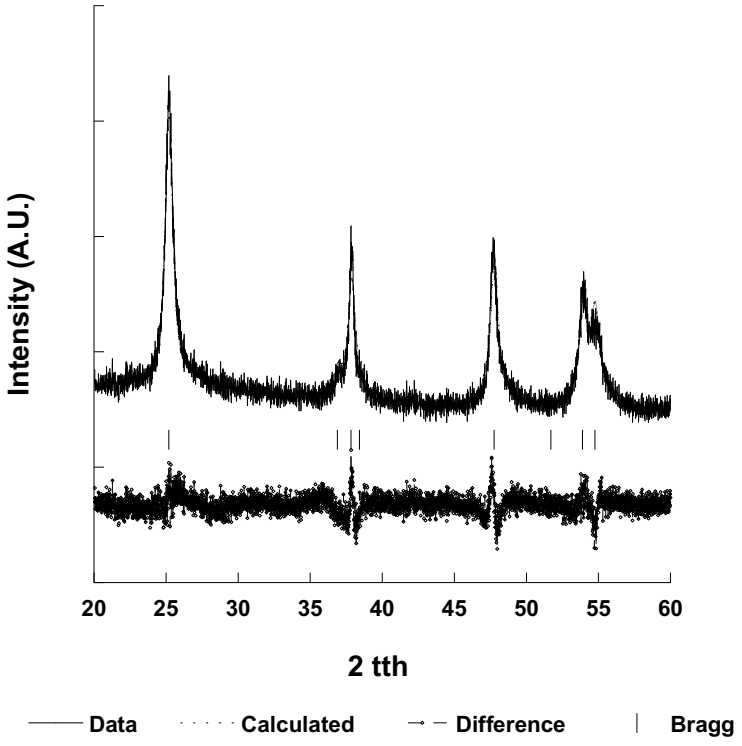

Figure 6: FullProf Fitting of the Anatase Diffraction data obtained at the 100°C 8 hr Reflux using sodium sulfate.

The average grain size of the synthesized nanomaterials was determined from the diffraction patterns using Scherrer's equation, which is shown below:

$$d = \frac{K\lambda}{\beta cos\frac{2\theta}{2}}$$

Where d is the average diameter of nanoparticle, K is a constant related to the Gaussian fitting of the diffraction patter and is 0.9, λ is the wavelength of the X-ray source used for the data collection, β is the full width half maximum of the diffraction peak, and cos 2θ/2 is the angel of diffraction. From the fitting of the diffraction peaks it can be seen in Table 4 the nanoparticles were in the range of 12-13 nm, the averages grain sizes of the nanoparticles were very close to each other.

Table 4: Average Grain Size of the Different TiO_2 Materials Synthesized, Determined by using Scherer's Equation.

Phase	Average Grain Size
Rutile	11.8
Brookite	13.1
Anatase	12.6

RAMAN

Figure 7, shows the RAMAN spectra collected for the synthesized samples for the brookite and anatase samples as the purity of these samples was unknown. RAMAN spectra allows for the determination of low levels of contamination. The spectra resemble those presented in the literature for the anatase and brookite phases [11,12]. The brookite shows Raman stretches at 128, 153, 247, 322, 366, and 636 cm^{-1} which has been published for this crystal system [11,12]. Whereas the anatase sample shows sharp RAMAN peaks at 146, 396, 515, and 641 cm^{-1} [11,12]. Neither of the anatase or brookite samples had the reported RAMAN peaks for rutile. The rutile peaks occur at 143, 235, 447 and 612 cm^{-1} [11,12]. The Raman data corroborate the data collected from the XRD studies indicating that synthesized anatase and brookite were pure and obtained under the reaction conditions at 100 °C.

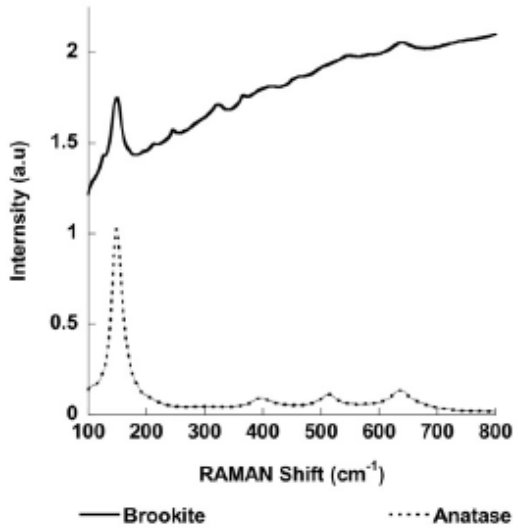

Figure 7: Raman Spectra of the Synthesized Anatase and Brookite Samples used for the Binding of Cr(III) and Cr(VI) from Aqueous Solution.

SEM

The SEM images of the as synthesized anatase, brookite and rutile nanoparticles are shown in Figure 8-10. The synthesized anatase begins to show some structure needle like particles are developed on top of very large cluster of small particles. The SEM of the brookite phase shows the material that was synthesized consisted of conglomerated clusters of small spherical particles. However, the SEM of the rutile nanoparticles, shows definite needle like structures. Overall the SEM of the rutile nanoparticles shows the clustering small needles into superstructures. The rutile phase superstructures appear truncated spherical structures.

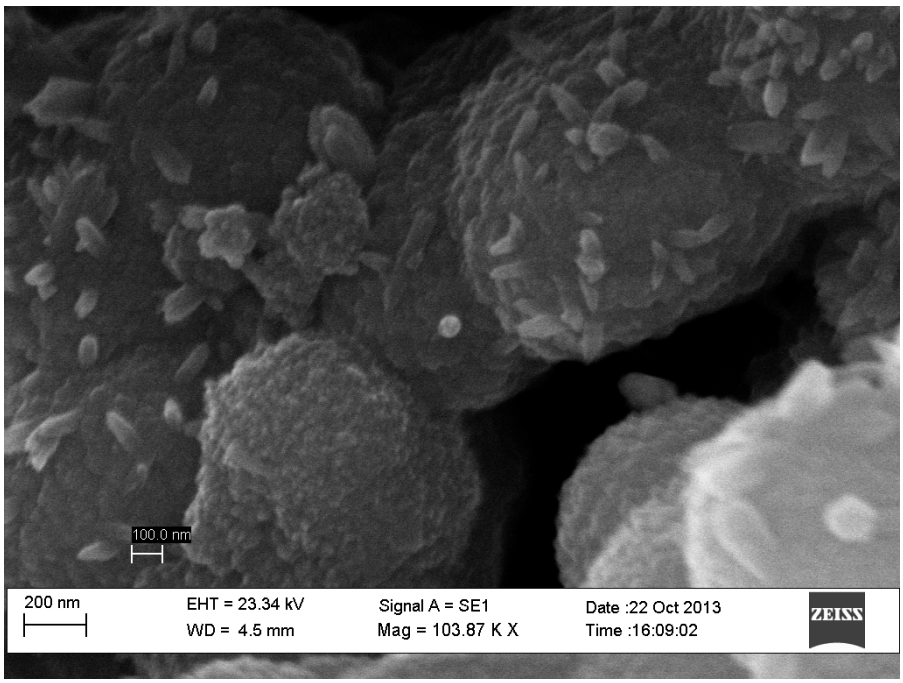

Figure 8: SEM image of the Hydrothermally Synthesized Anatase Nanoparticles.

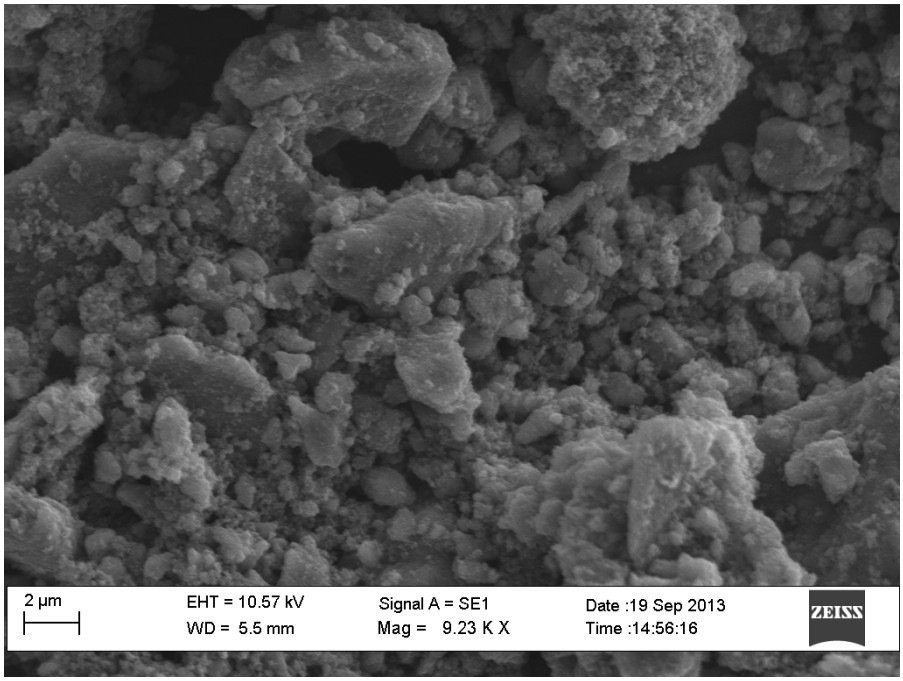

Figure 9: SEM images of the Hydrothermally Synthesized Brookite Nanomaterial.

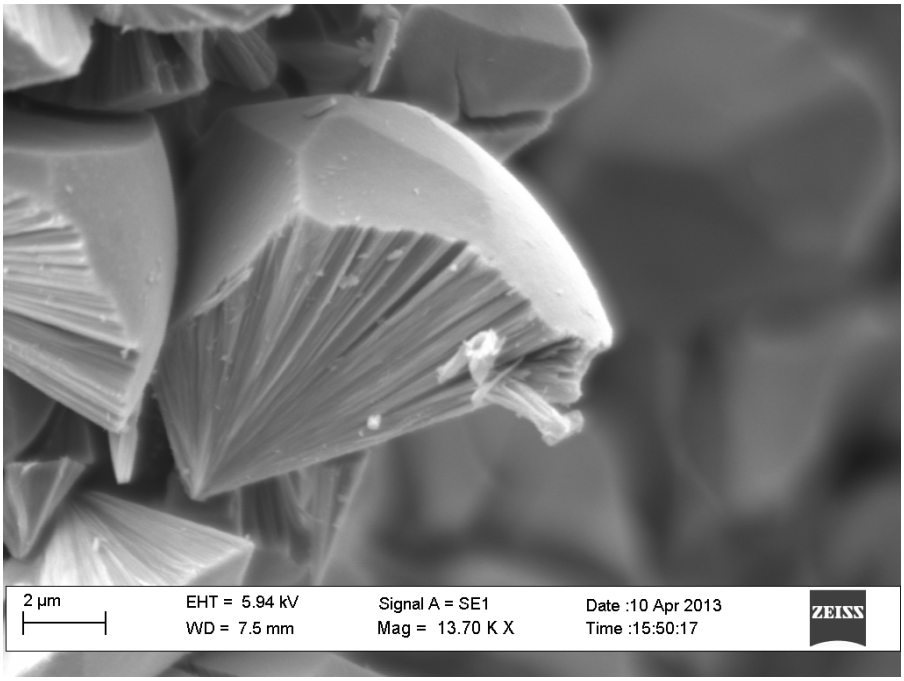

Figure 10: SEM image of the Rutile TiO_2 Nanoparticles Synthesized Hydrothermally at 110°C.

pH Profile

A significant factor that effects the binding of heavy metals onto nanomaterials has been shown to be the pH of the solution. In the present study, various pH's were investigated to determine the optimum binding pH for the removal of chromium (III) and chromium (VI) using the titanium dioxide polymorphs. In the present study chromium (III) and chromium (VI) solutions were prepared over a pH range of 2 through 6 and then added to anatase, brookite, or rutile nanomaterial to determine the optimum binding pH.

The sorption of Cr(III) and Cr(VI) onto the anatase polymorph is shown in Figure 11A. At low pH values, anatase removed very little Cr(III), however as the pH increased the percent bound to the nanomaterial increased as well. The optimum removal was achieved at pH of 4, with approximately 32% of the total Cr(III) removed. However, as the pH was increased further

the binding of Cr(III) was observed to decrease. Chromium (VI), on the other hand, showed a constant binding of approximately 80% at all the pH's studied. The constant binding observed for Cr(VI) indicates the binding of Cr(VI) to the anatase phase was pH independent. A pH of 4 was determined to be the optimum pH for the removal of both chromium (III) and chromium (VI) binding to the anatase polymorph.

The binding for Cr(III) and Cr(VI) with brookite can be seen in Figure 11B. The percent binding for Cr(III) was observed to be approximately 71% at pH 2 and 3. However, a pH of 4, the percent binging increased above 90% and remained constant as the pH was increased further. Chromium (VI) showed over 80% removal at a pH of 2 and the binding was observed to increase as the pH of the solution was increased. At pH 5, over 90% of chromium (VI) was removed by the nanomaterial. As a result, the optimum binding pH for the removal of Cr(III) and Cr(VI) by brookite was determined to be pH of 5.

The results for the rutile polymorph can be seen in Figure 11C, which removed very little Cr(III) at low pH's between 2 and 4 showing a percent binding ranging from 0.84% to 4%. At a pH of 5 and 6, the binding spiked up to 32% and 39% respectively. In contrast, the binding of chromium (VI) onto rutile appeared to remain constant throughout the study with increasing pH. At a pH of 2, approximately 95% of the metal Cr(VI) had bound and as the pH increased so did the binding of the Cr(VI) increased slightly. The optimum pH selected for both chromium (III) and chromium (VI) was determined to be pH 5.

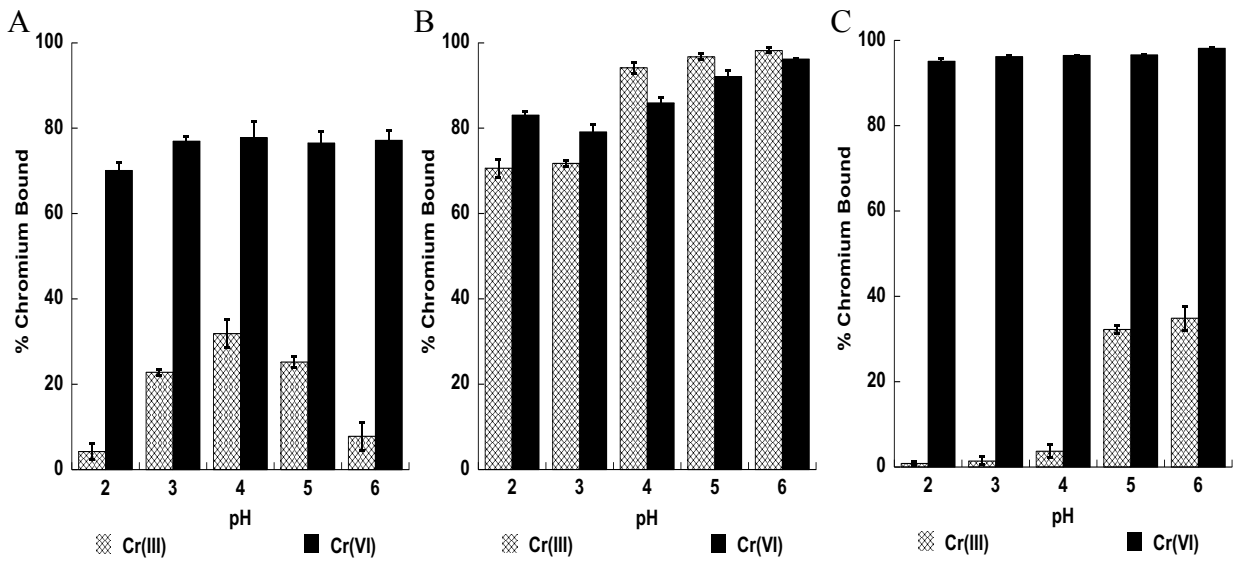

Figure 11: Effects of pH on the Binding of Cr(III) and Cr(VI) with TiO_2 Polymorphs A) Anatase, B) Brookite, C) Rutile.

Overall, the results for the pH studies show a trend in which the binding increases as the pH increases, with the exception of the Cr(III) binding to the anatase nanophase. The results for all the polymorphs appear to follow an opposite trend compared to many other metal oxides studied for the removal of chromium(VI) ions. However, the chromium(III) binding followed similar trends observed in the literature. For example, Cantu et. al, used Mn_3O_4 for the removal of both Cr(III) and Cr(VI) which exhibited a decrease in removal with increasing pH [7]. The same trend as in the present study was observed by Luther et al., using Fe_3O_4 and $MnFe_2O_4$ nanomaterials for the binding of both Cr(III) and (VI) ions [9]. pH trends observed in the literature show the optimum pH similar between pH 4 and pH 6 for chromium(III) binding and Cr(VI) [7,9].

Time/ Kinetics Studies

The results of the time dependency and kinetics studies are presented in Table 5 for the Cr(III) and Cr(VI) binding to the three phases of TiO_2. The kinetics data were determined by

plotting the percentage of chromium bound in solution as a function of time. A plot was developed which had the following equation:

$$\%B = Kt$$

Where %B is the percent of the chromium species bound to the nanomaterial, K is the rate constant for the reaction, and t is the time in minutes. The reaction was determined to follow first order kinetics. First order kinetics can be defined from a plot of the concentrations against time if a linear relationship is observed.

As can be seen in the data present in Table 5, the trend is an increase in the slope of the line with increasing temperature. The data indicates that reaction is an endothermic reaction. The rate of the reaction is increasing with increasing temperature. For the most part, the rate of the reaction rate doubles or triples with the increase in temperature for binding of both Cr(III) and Cr(VI) to the different TiO_2 nanomaterials. The increasing rate of binding with increasing temperature has been observed in the literature for a number of different metal binding studies. The binding of Cr(VI) to the Brookite nanomaterial shows only a very small increase in the rate of binding from 0.3484 to 0.3573. Of the materials studied, the Brookite Cr(VI) has the smallest change in rate with increasing temperature, which indicates the process is temperature independent. The temperature independence indicates that the reaction would more than likely go through an ion exchange type mechanism.

Table 5: Summary of the Kinetics for the Binding of Cr(III) and Cr(VI) to Anatase, Brookite, and Rutile.

TiO_2 Phase	Cr ion	Temp. (K)	Equation	R^2	E_a (kJ/mol)
Anatase	Cr(III)	280	0.0138X+1.22	0.962	12.89
		295	0.02x+3.48	0.971	
		318	0.0268x+3.41	0.982	
	Cr(VI)	280	0.0707+4.88	0.994	23.05
		295	0.1195x+14.63	0.985	
		318	0.2313x+15.44	0.994	
Brookite	Cr(III)	280	0.0263x+1.26	1.00	22.75
		295	0.0322x+0.79	0.997	
		318	0.0789+4.11	0.994	
	Cr(VI)	280	0.3484X+34.64	0.980	0.48
		295	0.3522x+74.95	0.997	
		318	0.3573x+74.75	0.993	
Rutile	Cr(III)	280	0.0267x+5.60	0.995	23.24
		295	0.0387x+0.93	0.980	
		318	0.0869x+6.78	0.980	
	Cr(VI)	280	0.189X+86.18	0.991	17.35
		295	0.263x+90.26	0.998	
		318	0.459X+79.55	0.998	

Activation Energy Studies

The activation energy studies were performed based on the data collected kinetics studies at different temperature. Arrhenius plots were developed using the changing rate constants for the reactions observed at the different temperatures. The Arrhenius equation in linear form is given below:

$$Ln(k) = -\frac{E_a}{RT} - Ln(A)$$

Where k is the rate constant, E_a is the activation energy, R is the gas constant 8.314 J mol^{-1} K^{-1}, T is the temperature given in Kelvin, and the A is a frequency factor. By plotting the natural log of the rate constant determined for the reactions at each temperature against the inverse of the temperature (K^{-1}) the Arrhenius plot is developed. Where the slope of the line is the negative

activation energy of the reaction divided by the gas constant. The Arrhenius plots for the binding of r(III) and Cr(VI) to the anatase, brookite, and rutile nanoparticles are shown in Figures 12, 13, and 14, respectively.

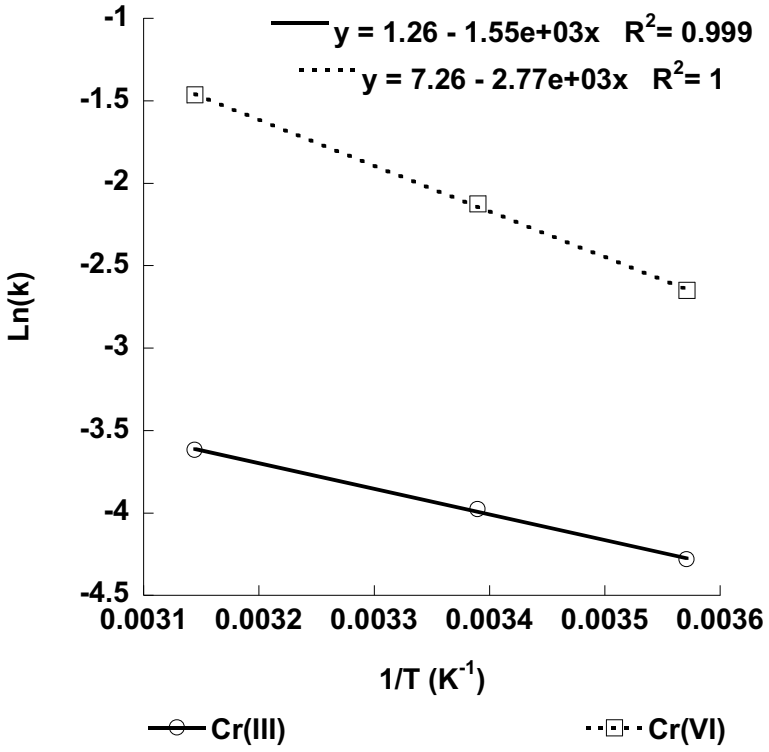

Figure 12: Arrhenius Plot for the Binding of Cr(III) and Cr(VI) to the Anatase Nanomaterial from 277K to 318K.

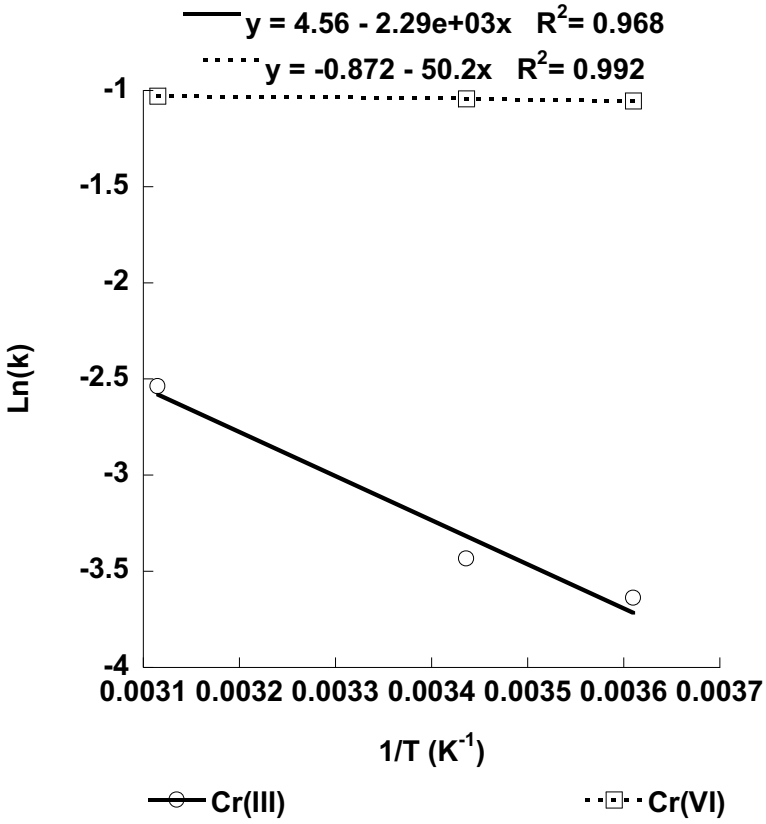

Figure 13: Arrhenius Plot for the binding of Cr(III) and Cr(VI) to the Brookite Nanomaterial from 277K to 318K.

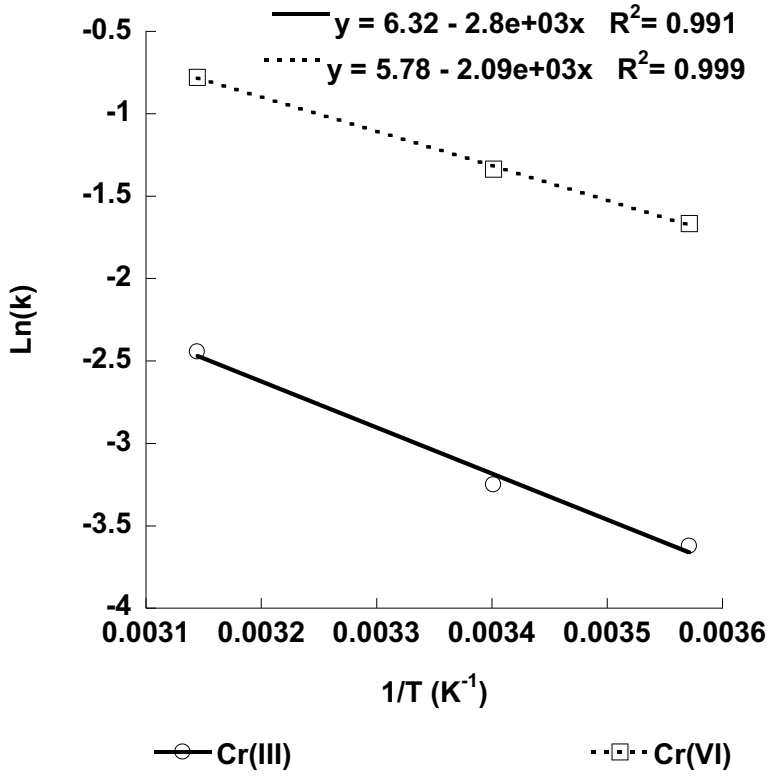

Figure 14: Arrhenius Plot for the Binding of Cr(III) and Cr(VI) to the Rutile Nanomaterial from 277K to 318K.

The calculated activation energies for the binding of both Cr(III) and Cr(VI) to the TiO_2 nanomaterials are shown in Table 5 with the kinetics data. As can be seen in Table 5 all the determined activation energies are positive and are variable in magnitude. The binding of Cr(III) to the anatase, brookite, and rutile nanomaterials had activation energies of 12.89, 22.75, and 23.24 kJ/mol. The magnitudes of these activation energies indicate that the reaction is occurring through ion-exchange/ physisorption. It has been shown in the literature that activation energies below 8 kJ/mol are indicative of an ion exchange, whereas activation energies in the range of 8

to 25 kJ/mol indicate physisorption [13,14]. And activation energies in the range of 25 to 83.7 kJ/mol indicate the reaction is going through chemisorption [13,14]. The binding of Cr(VI) to the anatase and rutile phases showed activation energies of approximately 23 kJ/mol, indicating the binding was occurring through physisorption. However, the activation energy for Cr(VI) binding to brookite was very low 0.48 kJ/mol which is in the range of ion exchange.

Capacity Studies

The maximum binding capacity for each nanomaterial used for the removal of chromium (III) and chromium (VI) was determined by using isotherm binding capacity studies, performed at 277 K, 295 K, and 318 K. Both the Cr(III) and Cr(VI) capacity studies were observed to follow the Langmuir isotherm. The linear form of the Langmuir isothermal model was used to determine the binding capacity for each of the titanium dioxide polymorphs. The linear form of the Langmuir isotherm equation is shown below:

$$\frac{1}{Q_e} = \frac{1}{K_a q_m C_e} + \frac{1}{q_m}$$

Where $Q_{e,}$ is the amount of metal bound to the material at a given concentration once equilibrium has been established, q_m is the binding capacity of the nanomaterial for the adsorbate, and C_e is the equilibrium concentration of the solution after being exposed to the adsorbent. K_a is the inverse of the distribution coefficient between the aqueous and solid phase. The binding capacities for Cr(III) and Cr(VI) binding to anatase, brookite, and rutile were determined by plotting Q_e^{-1} vs. C_e^{-1}. The generated plots had correlation coefficients (R^2) of 0.99 or better. The linear fits of the plats were used to determine the binding capacity from the intercept ($1/q_m$) and the slopes of the fittings were $1/K_{d,}$ which is the inverse of the distribution coefficient. The

determined distribution coefficients were further used to determine the thermodynamics of the binding process.

Based on the results shown in Tables 6-8, rutile had the highest binding capacity for Cr(III) at room temperature with a binding capacity of 11.2 mg/g, at a temperature of 295 K. However, brookite had the highest binding capacity for Cr(VI) at this temperature with approximately 15.5 mg/g bound at a temperature of 295 K.

From Table 6-8, it can be seen that for anatase, as the temperature increases the capacity for Cr(III) binding increased. For example, at 277 K, the binding for Cr(III) was 6.03 mg/g, and at 295˚K, it decreases to 1.86 mg/g and by 318 K, the binding capacity increases to 9.08 mg/g. The binding capacity trend observed for the Cr(VI) binding to the anatase polymorph showed a continual binding increase with increasing temperature. The Cr(VI) binding at 277 K was 1.81 mg/g and increased at 295 K to 9.17 mg/g. The binding capacity for Cr(VI) increased further at 318 K to 10.72 mg/g. For the brookite binding a similar trend was observed for Cr(III) the binding started at 6.99 mg/g at 277 K and increasing to 8.77 mg/g at 318 K. However, the binding of the Cr(VI) to the brookite showed the opposite trend with decreased binding with increased temperature. The Cr(VI) binding to the brookite was 16 mg/g at 277 K and decreased to 14.37 mg/g at 318 K. Both the binding of Cr(III) and Cr(VI) showed increasing binding with increasing temperature. The Cr(III) binding was 8.29 mg/g at 277 K and increased to approximately 20 mg/g at 318 K. Whereas the Cr(VI) has a binding of 9.84 mg/g at 277 K and increased to 16.83 at a temperature of 318 K.

Table 6: Adsorption Capacities for the Binding of Cr(III) and Cr(VI) with the Anatase Polymorph.

Polymorph	Ion	Temperature (K)	Capacity (mg/g)
Anatase	Cr(III)	277	6.03
		295	1.86
		318	9.08
	Cr(VI)	277	1.81
		298	9.17
		318	10.72

Table 7: Adsorption Capacities for the Binding of Cr(III) and Cr(VI) with the Brookite Polymorph.

Polymorph	Ion	Temperature (K)	Capacity (mg/g)
Brookite	Cr(III)	277	6.99
		295	7.10
		318	8.27
	Cr(VI)	277	16.00
		298	15.15
		318	14.37

Table 8: Adsorption Capacities for the Binding of Cr(III) and Cr(VI) with the Rutile Polymorph.

Polymorph	Ion	Temperature (K)	Capacity (mg/g)
Rutile	Cr(III)	277	8.29
		295	11.12
		318	20.04
	Cr(VI)	277	9.84
		299	11.78
		316	16.83

The results obtained in the present study for the binding capacity of chromium (III) onto the titanium dioxide polymorphs was significantly lower compared to other adsorbents in the literature. Literature values for adsorbents removing chromium (III) ranged between 19-41 mg/g, which prove to be more successful in its removal. For chromium (VI), the binding

capacity for the titanium dioxide polymorphs were very similar to literature values in which literature values for other adsorbents ranged from 0.5-21 mg/g. Additionally, large variations in the binding capacities can be attributed to multiple factors, such as particle size, porosity, and material stability.

Isotherms

The Gibbs free energy for the adsorption of chromium III and chromium VI onto the titanium dioxide polymorphs anatase, brookite, and rutile were calculated using the following equation:

$$\Delta G = -RT\ln K_d$$

where ΔG is the Gibbs free energy, R is the ideal gas constant (8.314×10^{-3} kJ mol^{-1}), T is the temperature in degrees Kelvin, and K_d is the distribution coefficient at that temperature. The ΔG values for the adsorption of chromium(III) and chromium(VI) onto anatase, brookite, and rutile are shown in Tables 9-11. The ΔG for the sorption of chromium(III) onto anatase was approximately 12.8 kJ/mol for temperatures between 277˚K to 318˚K respectively. Whereas the ΔG for binding of Cr(III) to the brookite nanomaterial ranged from 6 to 9.3 kJ/mol in the temperature range from 277 K to 318 K. The ΔG for the adsorption of Cr(III) onto rutile were in the range of 8.8-8.5 kJ/mol from temperatures of 277 K to 318 K. Based on the positive Gibbs Free Energy values, it can be concluded that the adsorption of Cr(III) onto the titanium dioxide polymorphs is non-spontaneous. In addition, the binding to the brookite nanophase was also exothermic in nature with the ΔG increasing with increasing temperature. Whereas the binding to the anatase and rutile phases was endothermic with only very small decrease in the ΔG with increasing temperature.

The ΔG values for the adsorption of chromium (VI) onto anatase, brookite, and rutile are shown in tables 9-11. The ΔG for the sorption of chromium (VI) onto anatase ranged from 1.81 kJ/mol to 10.72 kJ/mol for temperatures between 277˚K to 318˚K respectively. The ΔG for the adsorption of Cr(VI) onto brookite had a range of -1.31 kJ/mol to -3.04 kJ/mol for temperatures between 277 ˚K to 318 ˚K respectfully. Lastly, rutile had a range of -0.22 kJ/mol to -2.28 kJ/mol for temperatures between 277 ˚K to 318 ˚K respectfully. Based on the positive Gibbs Free Energy value for the sorption of Cr (VI) onto anatase it can be concluded that the process is non-spontaneous. The sorption of Cr(VI) onto brookite and rutile on the other hand, had negative values which indicate that the process is spontaneous.

Thermodynamic studies for the sorption of both Cr(III) and Cr(VI) has been extensively studied in the literature with many metal oxides. For example, Cantu et al. studied the thermodynamics of Cr(III) and Cr(VI) to Mn_3O_4 nanomaterial. For the binding of Cr(III) to manganese oxide, the ΔG values had a range of -2.9 to -23.7 kJ/mol, and the binding of Cr(VI) onto the same material had a range of -0.9 to -3.9 kJ/mol. Additionally, Luther et al. found that the binding of Cr(III) onto $MnFe_2O_4$ had a range of -17.16 and -11.40 kJ/mol, whereas Cr(VI) had a range of -7.5 to -7.02 kJ/mol. All of these literature values are negative and indicate that the adsorption process is spontaneous and exothermic.

The enthalpy and entropy for the adsorption of chromium(III) and chromium (VI) onto anatase, brookite, and rutile was calculated using the following equation:

$$\Delta G = \Delta H - T\Delta S$$

where ΔG is the Gibbs free energy, ΔH is the change in enthalpy, T is the temperature in degrees Kelvin, and ΔS is the change in entropy. The equation above can be re-written using the K_d distribution coefficient as follows:

$$-RT\ln K_d = \Delta H - T\Delta S$$

where it can then be rearranged to form a linearized relationship between the following variables K_d, ΔH, and ΔS. The rearranged equation is listed below

$$Ln(K_d) = \frac{\Delta S}{R} - \frac{\Delta H}{RT}$$

from the equation above, $\ln K_d$ is plotted versus 1/T where the slope of the trend line is $-\frac{\Delta H}{R}$ and the y-intercept is $\frac{\Delta S}{R}$. The plots for the thermodynamic determination are shown in Figures 15 to 17.

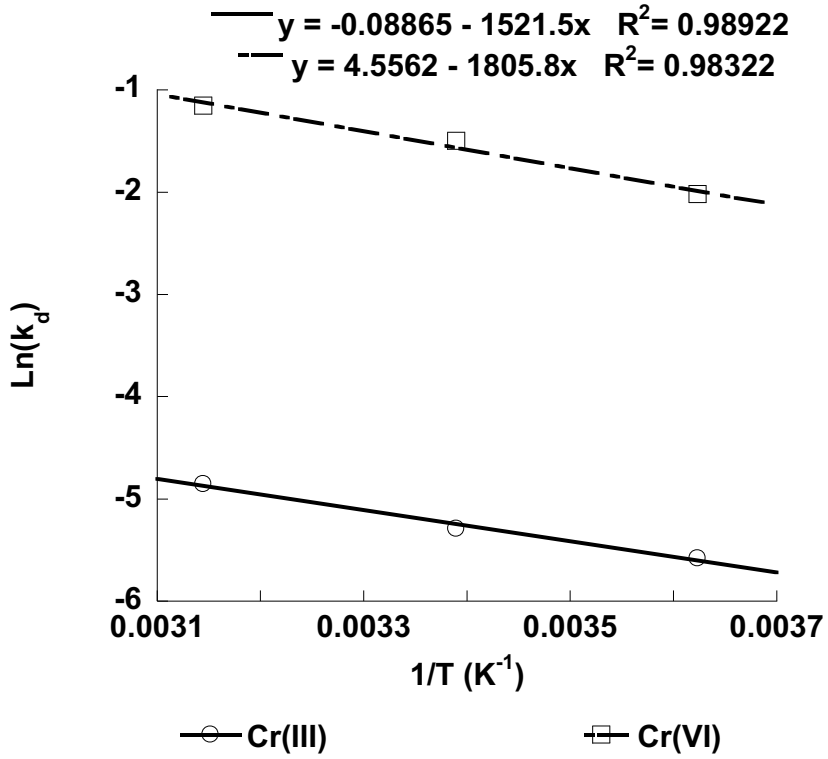

Figure 15: Thermodynamics Plot for the Binding of Cr(III) and Cr(VI) to the Anatase Polymorph of TiO_2 at Temperatures of 277, 295 and 318K.

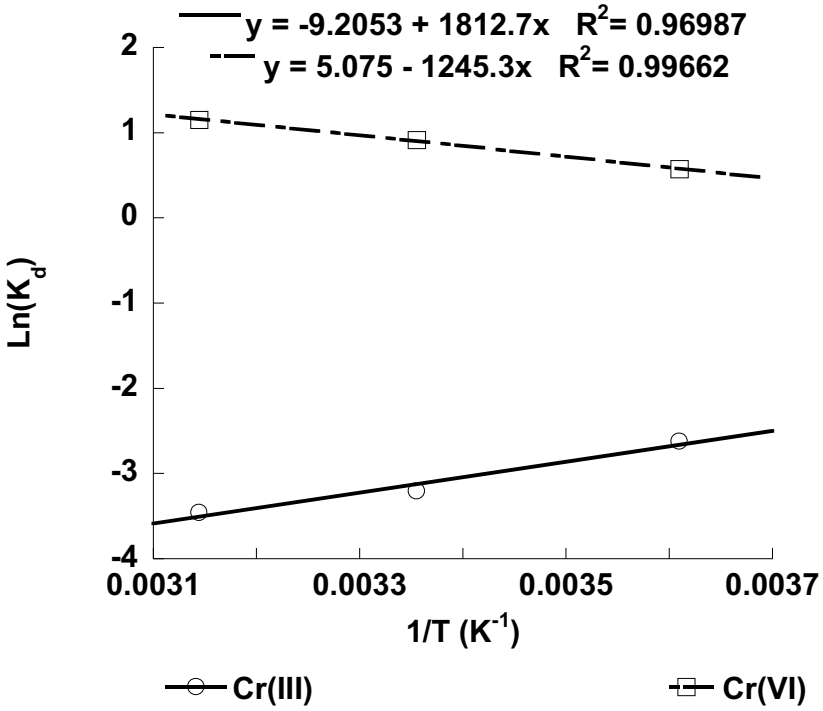

Figure 16: Thermodynamics Plot for the Binding of Cr(III) and Cr(VI) to the Brookite Polymorph of TiO_2 at Temperatures of 277, 295 and 318K.

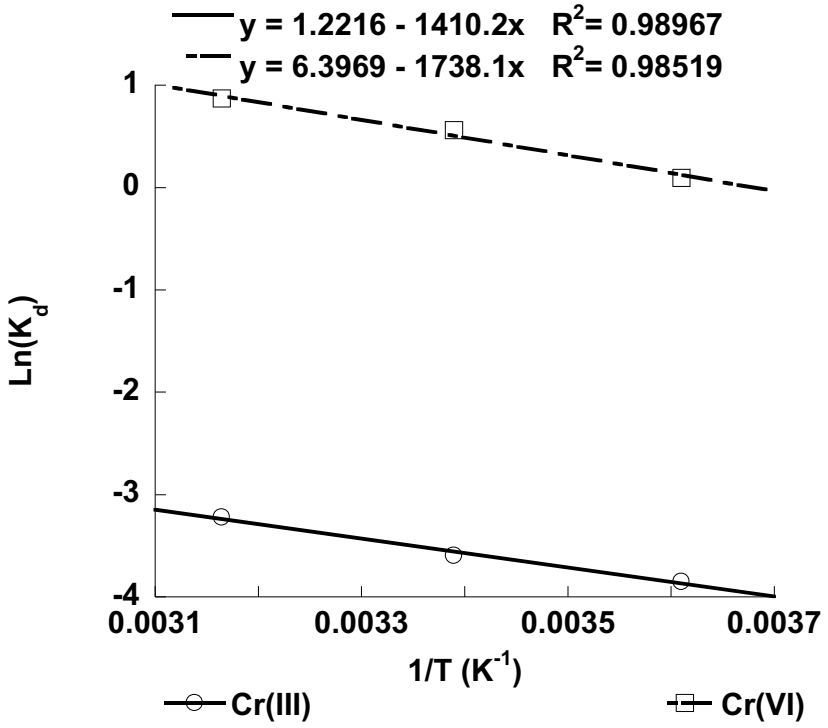

Figure 17: Thermodynamics Plot for the Binding Cr(III) and Cr(VI) to the Rutile Polymorph of TiO_2 at Temperatures of 277, 295 and 318K.

Both the enthalpy and entropy were calculated using trend lines with correlation coefficients containing a 0.96 or better. Furthermore, the calculated values for ΔH and ΔS are shown in Tables 9,10, and 11 for anatase, brookite, and rutile respectively.

Table 9: Thermodynamic Parameters for the Sorption of Cr(III) and Cr(VI) with the Anatase Polymorph.

Polymorph	Ion	Temperature (K)	ΔG	ΔH	ΔS
Anatase	Cr(III)	277	12.89	13.31	1.59
		295	12.84		
		318	12.83		
	Cr(VI)	277	1.81	16.94	43.92
		298	9.17		
		318	10.72		

Table 10: Thermodynamic Parameters for the Sorption of Cr(III) and Cr(VI) with the Brookite Polymorph.

Polymorph	Ion	Temperature (K)	ΔG	ΔH	ΔS
Brookite	Cr(III)	277	6.03	-17.08	-88.44
		295	7.94		
		318	9.29		
	Cr(VI)	277	-1.31	10.01	41.10
		298	-2.26		
		318	-3.04		

Table 11: Thermodynamic Parameters for the Sorption of Cr(III) and Cr(VI) with the Rutile Polymorph.

Polymorph	Ion	Temperature (K)	ΔG	ΔH	ΔS
Rutile	Cr(III)	277	8.86	11.24	8.44
		295	8.82		
		318	8.52		
	Cr(VI)	277	-0.22	23.27	94.58
		298	-1.39		
		318	-2.28		

The adsorption of chromium(III) onto anatase was calculated to have a ΔH of 13.31 kJ/mol and a ΔS of 1.59 J/mol. The adsorption of Cr(III) onto brookite was calculated to have a ΔH of -17.08 kJ/mol and a ΔS of -88.44 J/mol. Furthermore, the adsorption of Cr(III) on the rutile had a ΔH of 11.24 kJ/mol and a ΔS of 8.44 J/mol. The chromium(VI) binding to the anatase and rutile polymorphs was endothermic in nature. The ΔH values for the binding indicate the binding occurred through ion-exchange. It has been indicated in the literature that ΔH values between 8 and 16 represent ion exchange mechanism, whereas ΔH values from 16-40 are indicative of physisorption, and ΔH values above 40 are characteristic of chemisorption [16]. The binding of Cr(III) to the brookite phase of TiO_2 indicate that the reaction occurs through physisorption. The binding of Cr(VI) to the anatase, brookite, and rutile showed ΔH 16.94, 10.0

and 23.27 kJ/mol. Associated ΔS with the binding of Cr(VI) to the anatase, brookite and rutile polymorphs were 43.92, 41.1, and 94.58 J/mole, respectively. The ΔS values for the binding of chromium(VI) are all positive indicating an increase in the entropy of the system after binding. The binding to the anatase and brookite indicate the binding was occurring through ion exchange of the Cr(VI) Whereas, the binding of the Cr(VI) to the rutile polymorph was occurring through physisorption. These results correlate to literature values, for instance, a study conducted by Valle et al., proved that the sorption of Cr(III) and Cr(VI) onto $K_2Mn_4O_9$ was spontaneous throughout all temperatures tested. Furthermore, the enthalpy of adsorption for the study indicated an endothermic process which correlates to the current study [20].

Interferences

In this study, chromium (III) and chromium (VI) solutions were prepared containing various ions to model real water conditions. In addition, the study was designated to determine if hard cations and anions effect the binding of the Cr(III) and Cr(VI) ions onto the titanium dioxide nanomaterials.

The binding of chromium (III) ions in solutions, which contained sodium ions (Na^+), onto anatase was significantly affected. As seen in Figure 18A, at a concentration of 0.3 ppm of sodium the binding of chromium was less than 1 percent which was nearly a tenfold decrease in the binding. As the concentration of Na^+ in the solution was increased, the binding of chromium(III) was observed to increases as well. The maximum was observed when the concentration of sodium was 3ppm, and the percent binding of chromium(III) remained at approximately 3% and remained relatively constant thereafter. Similarly, the presence of K^+ in the solution effected the sorption of Cr(III) onto the anatase polymorph. At concentrations of 0.3 ppm, 3ppm and 30ppm of K^+ the percent binding of the chromium (III) ions to anatase was

approximately 3%. As the concentration of K^+ was increased so did the removal of Cr(III). At 100ppm of potassium, approximately 5% of the chromium (III) was bound to the nanomaterial, and the binding remained relatively constant thereafter. The binding of Cr(III) with anatase in the presence of 0.3 ppm of calcium was approximately 3% and remained rather constant up to a 30 ppm of calcium concentration. The binding was observed to increase to approximately 7% at a Ca^{2+} concentration of 30 ppm and remained relatively constant thereafter. The binding of Cr(III) to the anatase nanomaterial in the presence of Mg^{2+}, showed a synergistic effect in which the binding of chromium (III) increased from 2.6% to 7.0% binding. In the presence of 300 ppm of Mg^{2+}, the binding decreased to approximately 2% and was observed to increase to 6.8% in the presence of 1000ppm of Mg^{2+}.

The binding of chromium (VI) to anatase was investigated by creating various solutions containing various concentrations of commonly found anions in solution. The results presented in Figure 18B show the binding of Cr(VI) in the presence of different anions. The Cr(VI) binding the presence of Cl^- shows an antagonistic effect occurring between 0.3 ppm to 300 ppm of $Cl^-$where the binding of chromium (VI) ions decreases from 37.4% to 7.6%. In the presence of 1000 ppm of Cl^-, the binding of chromium (VI) observed to increase to 30%. In the presence of nitrate ions, chromium (VI) binding was observed to increase in binding. The presence of 0.3 ppm, 30 ppm, and 100 ppm and 300 ppm of NO_3^- showed an increase in binding from 26% to 47% in the presence of 1000 ppm of NO_3^-. In the presence of sulfate ions, the binding of Cr(VI) showed a decrease in the presence of SO_4^{2-} at concentrations of 0.3 to 30 ppm, from 41% to 31%. However, in the presence of 100 ppm of sulfate Cr(VI) binding increased to 40% then was observed to decrease at sulfate concentrations of 300 ppm and 1000 ppm to 29% and 2% respectively. In the presence of phosphate ions, chromium (VI) an antagonistic effect was

observed for the binding. The percent binding was observed to decrease with increasing concentrations of PO_4^{3-}. At 0.3 ppm, the binding is 43% but by 1000 ppm PO_4^{3-}, the binding was decreased to approximately 1%.

The combined interference study is shown in Figure 19 for both Cr(III) and Cr(VI) binding to the anatase nanomaterial. In the presence of all the cations the binding of Cr(III) was observed to increase with increasing concentrations of hard cations. However, the chromium(VI) in the combined anion interference solutions showed a decrease in the binding with increasing concentrations of the anions.

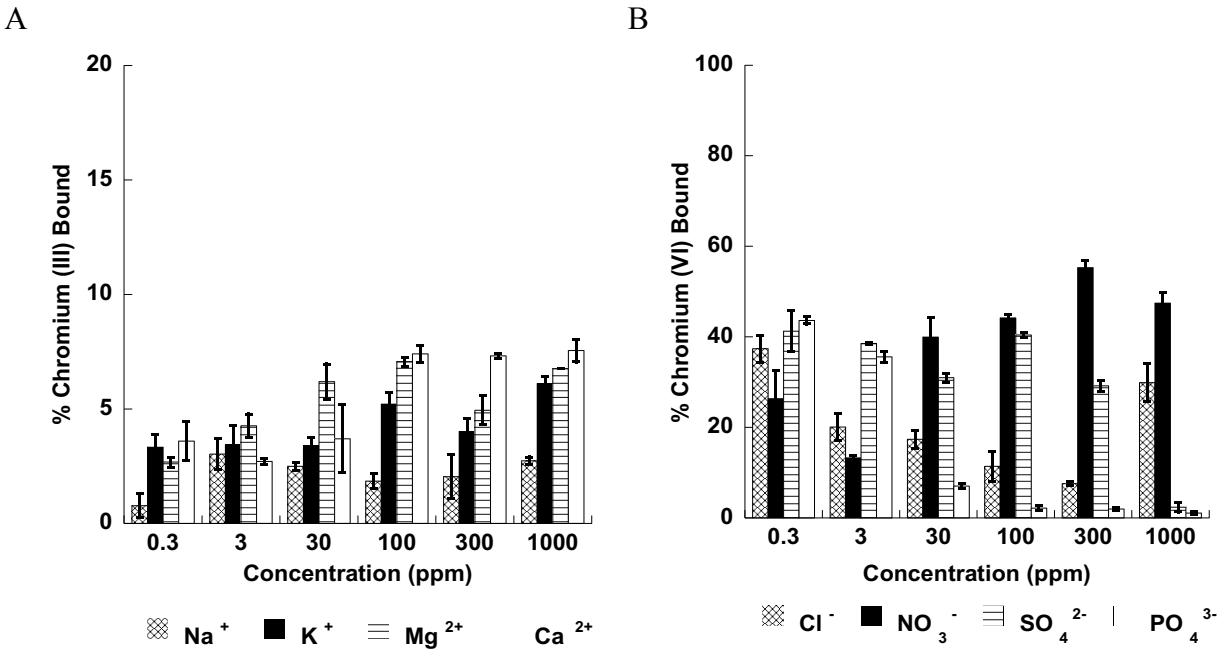

Figure 18: Effects of A) Na^+, K^+, Mg^{2+}, or Ca^{2+} on the Sorption of Cr(III), B) Cl^-, NO_3^-, SO_4^{2-}, or PO_4^{3-} on the Sorption of Cr(VI), with the Anatase Polymorph.

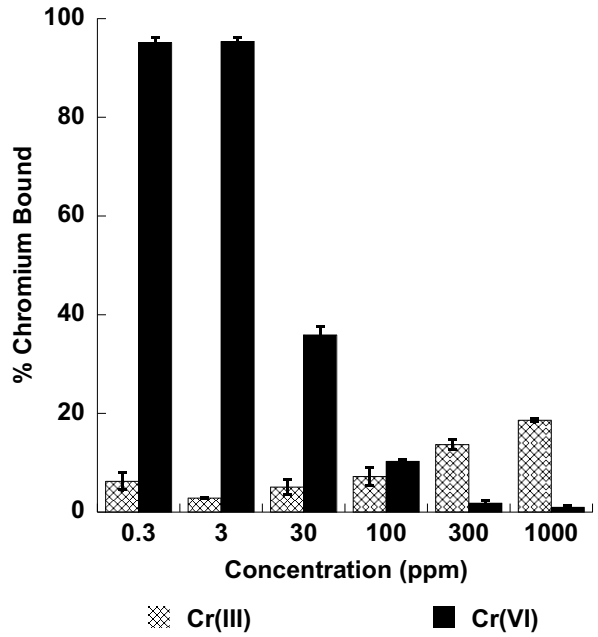

Figure 19: Effects of a Combination of the Interference ions on the Sorption of A) Cr(III) and B) Cr(VI) with the Anatase Polymorph.

The interference of common ions on the binding of Cr(III) and Cr(VI) to Brookite was also investigated using various ions to determine any possible interference on the binding. The interference on Cr(III) and Cr(VI) binding to the Brookite phase is shown in Figures 20 and 21. The results for the sorption of Cr(III) shown in Figure 20A, which show the presence of Na^+ had a negative effect on the binding of Cr(III) to the Brookite nanomaterial. Brookite in the presence of a Na^+ concentration of 0.3 ppm only 3.5% of chromium (III) was bound. Additionally, as the concentration of Na^+ increased to 3 ppm and 30 ppm, the binding decreased to 1.34% and 1.22%, respectively. However, as the Na^+ concentration increased to 100 ppm, 300 ppm, and 1000 ppm, the binding increased slightly to 2.94%, 4.62%, and 6.93%, respectively. The presence of potassium however, at all concentrations, negatively affected the binding of Cr (III). In solutions containing 3 ppm of K^+, the binding of Cr(III) to brookite was 1.39%. At a concentration of 3 ppm K^+, the binding slightly increased to 2.54% then observed to decrease with increasing

concentration of K^+ at concentrations of concentrations: 30 ppm and 300 ppm to the binding was observed to be 1.71% and 1.49%, respectively. Then a slight increase was observed at 1000 ppm K^+ concentration with a binding of 8.37%. The sorption of Cr(III) in the presence of 0.3 ppm of Mg^{2+} showed a binding of approximately 10%. However, a slight decrease to 8% was then observed at a Mg^{2+} concentration of 3 ppm. Increasing the concentration of Mg^{2+} showed a synergistic effect on the binding of Cr(III) and the binding reached its maximum of 14% at 1000 ppm of Mg^{2+}. A similar trend was observed for the sorption of Cr(III) in the presence of Ca^{2+} in which the binding appeared to be around 3% with 0.3 ppm Ca^{2+}. Ca2+ concentrations of 3.0 and 30 ppm Ca^{2+} showed a slight decrease in the binding of the Cr(III). Between 100 and 1000 ppm Ca^{2+}, a synergistic effect was observed which showed a binding increased to a maximum of 12%.

Figure 20B shows that the sorption of Cr(VI) in solutions which contain anions which are commonly found in natural waters. The binding of Cr(VI) with Cl^- appears to be unaffected and remained constant with a removal of approximately 80% r throughout the study. Chromium (VI) in the presence of NO_3^- also appears to be unaffected and remained constant and a binding of approximately 80% was observed. Chromium (VI) in in solutions containing 0.3 ppm, 3 ppm, and 30 ppm of SO_4^{2-} showed an increase in the binding with removals of 85%, 86% and 90%, respectively. At sulfate concentrations 100 ppm, 300 ppm, and 1000 ppm the binding was observed to decrease to 66%, 46%, and 22%, respectively. In solutions containing the chromium (VI) with PO_4^{3-} at concentrations of 0.3 ppm and 3 ppm, the binding was observed to be approximately 90%. However, as the concentration of PO_4^{3-} increased to from 30 ppm to 1000 ppm, the binding of Cr(VI) was observed to decreases to a minimum of 15%.

The combined interference study is shown in Figure 21 for both Cr(III) and Cr(VI) binding to the anatase brookite nanomaterial. The binding observed in the combined interference study was very similar to the anatase combined interference study. In the presence of all the cations the binding of Cr(III) was observed to increase with increasing concentrations of hard cations. However, the chromium(VI) in the combined anion interference solutions showed a decrease in the binding with increasing concentrations of the cations.

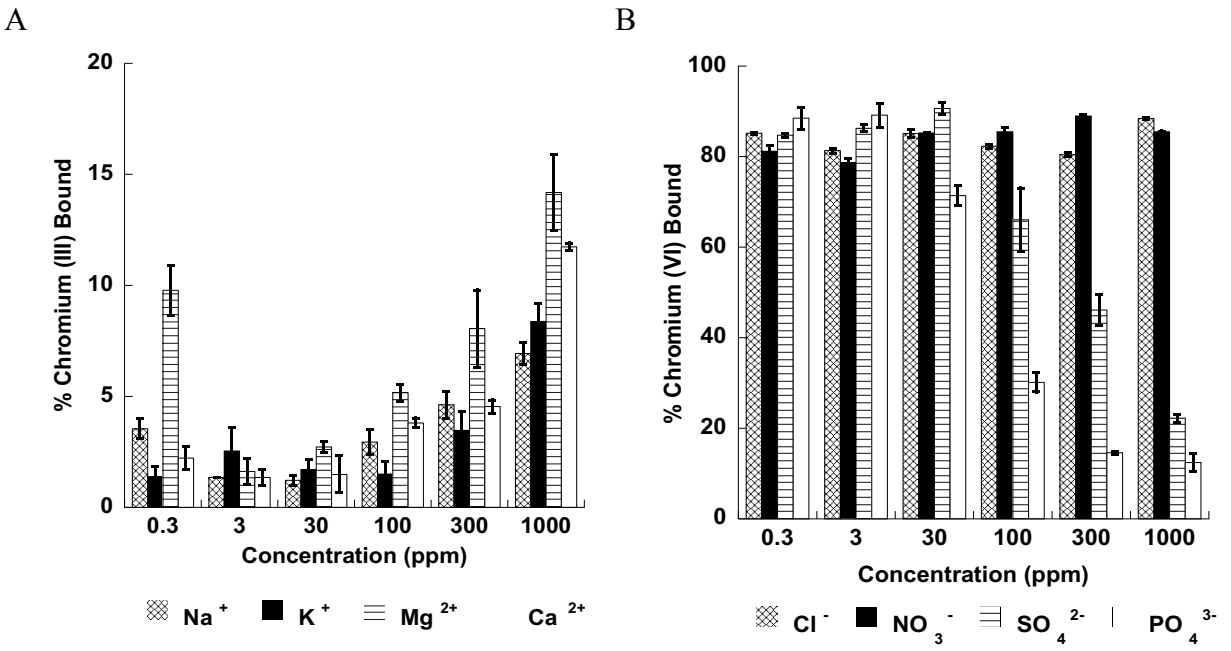

Figure 20: Effects of A) Na^+, K^+, Mg^{2+}, or Ca^{2+} on the Sorption of Cr(III), B) Cl^-, NO_3^-, SO_4^{2-}, or PO_4^{3-} on the Sorption of Cr(VI), with the Brookite Polymorph.

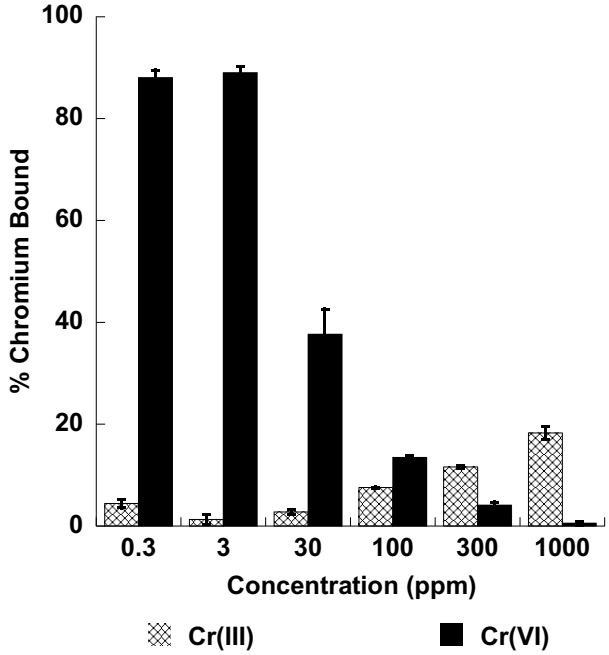

Figure 21: Effects of a Combination of the Interference Ions on the Sorption of A) Cr(III) and B) Cr(VI) with the Brookite Polymorph.

The binding of Cr(III) and Cr(VI) to rutile in the presence of commonly found cations and anions in natural water systems was investigated. The results for the single species interference and combined interference studies are for the sorption of Cr(III) and Cr(VI) are shown in Figures 22 and 23. The binding of chromium (III) in the presence of hard cations is shown in Figure 22A. As can be seen the binding remained constant between 1.7% and 2.4% for Na^+ concentrations of 0.3 ppm to 300 ppm. However, at 1000 ppm Na^+ concentration had a slight increase to 6% binding was observed. In solutions containing K^+ the binding of Cr(III) was inhibited. At 0.3ppm of K^+, the percent bound was 2.12%. As the concentration of K^+ increased to 3 ppm, 30 ppm, and 100 ppm the percent binding was observed to decreases to 1.68%, 1.78%, and 0.66%, respectively. However, at concentrations of K^+ from 300 ppm to 1000 ppm, a slight increase was observed in the binding from 2% to 4.7% respectively. In the presence of 0.3 ppm of Ca^{2+}, rutile had showed a 9.22% binding of the chromium (III). At Ca^{2+}

concentrations of 3 ppm to 100 ppm, the percent bound remained relatively constant at approximately 2%. At higher Ca^{2+} concentrations of 300 ppm to 1000 ppm, percent Cr(III) bound was observed to increase to 7% and 12%, respectively. The presence of Mg^{2+} in the binding solution at a concentration of 0.3 ppm showed approximately 13% binding of chromium (III). A decrease in the Cr(III) was observed a Mg^{2+} concentration of 3 ppm with a percent bound to approximately 2%. As the Mg2+ concentrations were increased to concentrations of 30 ppm, 100 ppm and 300 ppm and 1000 ppm the percent Cr(III) increased to 3.5%, 7.8%, 9.6%, to 17.2%, respectively.

The effects of the anion interferences on the sorption of Cr(VI) with rutile are shown in Figure 22B. In the presence of Cl^- the binding of Cr(VI) appeared to be unaffected with a 96% or greater binding observed throughout the study. In addition, the sorption of Cr(VI) from solution containing NO_3^- were also unaffected showing percent bindings of 97% or greater. In the presence of 0.3 ppm for SO_4^{2-}, chromium (VI) had a binding of approximately 96%. When the concentration of sulfate was increased to 3ppm the binding of Cr(VI) slightly increased to 99.6% binding. As the sulfate concentration increased to 30ppm, 100ppm, 300ppm, and 1000ppm the binding of Cr(VI) slowly decreases to 95%, 89%, 68.9%, and 59%, respectively. The binding of the Cr(VI) in the presence of PO_4^{3-} at concentrations of 0.3 ppm and 3 ppm was observed to be approximately 94%. However, as the concentration was increased to 30 ppm, 100 ppm, 300 ppm, and 1000 ppm the percent binding was observed decreased to 47%, 14%, 7%, and 5% respectively.

The combined interference study is shown in Figure 23 for both Cr(III) and Cr(VI) binding to the rutile nanomaterial. The binding observed in the combined interference study was very similar to both the anatase and brookite combined interference study. In the presence of all

the cations the binding of Cr(III) was observed to increase with increasing concentrations of hard cations. However, the chromium(VI) in the combined anionic interference solutions showed a decrease in the binding with increasing concentrations of the cations.

The results from the current study are similar of those presented by Valle et al., in which the sorption of Cr(III) increased with an increase in interfering cation concentration with the exception of the presence of Mg^{2+} and Na^{+} which inhibited the binding at higher concentrations. Furthermore, the sorption of Cr(VI) appeared to decrease as the concentration of the anions increased [20].

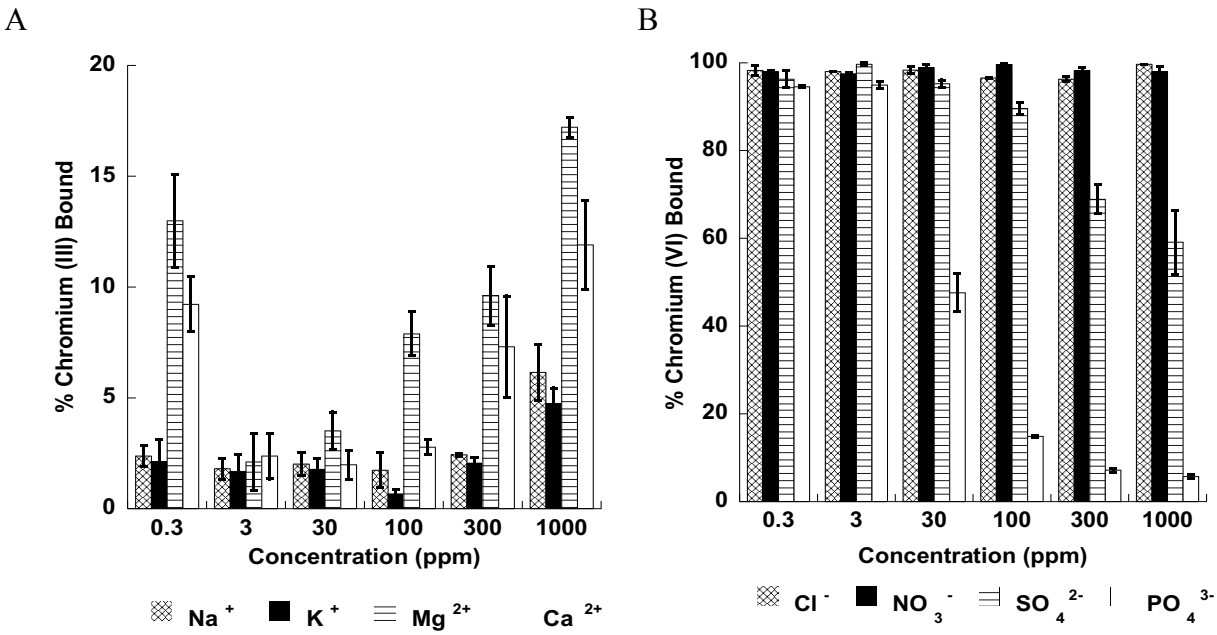

Figure 22: Effects of A) Na^{+}, K^{+}, Mg^{2+}, or Ca^{2+} on the Sorption of Cr(III), B) Cl^{-}, NO_3^{-}, SO_4^{2-}, or PO_4^{3-} on the Sorption of Cr(VI), with the Rutile Polymorph.

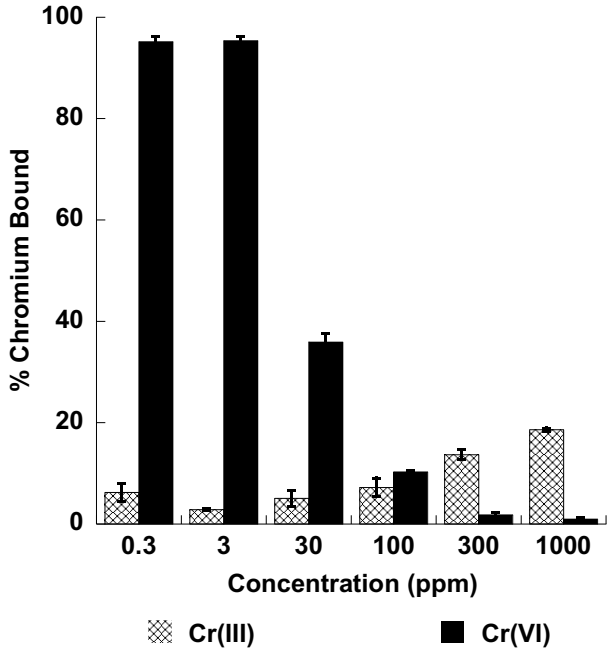

Figure 23: Effects of a Combination of the Interference Ions on the Sorption of A) Cr(III) and B) Cr(VI) with the Rutile Polymorph.

CHAPTER IV

CONCLUSIONS

A reflux synthesis method was employed for the synthesis of Anatase and Brookite, which produced the correct polymorph phases with an average particle size of 12.6 nm and 13.1 nm, respectfully. Rutile on the other hand, was synthesized through a hydrothermal method which produced pure nanomaterial that had an average particle size of 11.8 nm.

The pH profile was used to determine the optimal pH for the binding of Cr(III) and Cr(VI) onto the titanium dioxide polymorphs. For anatase, it was found that the binding of Cr(III) was negatively inhibited at low pH's and as the pH increased, so did the binding. The optimum was determined to be a pH of 4 with a binding of 32%. Cr(VI) on the other hand, had a constant binding of approximately 80% throughout the entire study, which proved to be pH independent. The binding of chromium (III) and chromium (VI) onto brookite appeared to favor higher pH's. For example, at a pH of 4 and above, the binding of Cr(III) appears to remain constant with a binding above 90%. Additionally, Cr(VI) had over 80% removal at a pH of 2, and the removal continued to increase with increasing pH. The optimum pH chosen for both ions was pH 5. Lastly, the optimum pH for the binding of Cr(III) and Cr(VI) onto rutile was pH 5. At this pH Cr(III) had a 32% removal and Cr(VI) had a removal greater than 95%.

Moreover, kinetic studies indicate that the reactions for the sorption of Cr(III) and Cr(VI) onto the polymorphs is endothermic and furthermore, the rate of the reaction appears to increase with increasing temperature. Of the materials studied, the sorption of Cr(VI) onto brookite had

the smallest change in rate with increasing temperature, which indicates that the process is temperature independent. Moreover, this indicates an ion exchange type of mechanism.

The activation energy was calculated from the data collected for the kinetic studies. All of the calculated energies are positive and variable in magnitude. The binding of Cr(III) onto anatase, brookite, and rutile had activation energies of 12.89, 22.75 and 23.24 kJ/mol. Furthermore, these values indicate that the reactions are occurring through ion exchange/physiorption. The binding of Cr(VI) onto anatase and rutile had energies of approximately 23 kJ/mol, which indicates that the process binding was occurring through physiorption. Lastly, the activation energy for the binding of Cr(VI) onto brookite was 0.48 kJ/mol which indicates that the binding is occurring through an ion exchange.

The maximum binding capacity for each nanomaterial used for the removal of chromium (III) and chromium (VI) was determined by using isotherm binding capacity studies, performed at 277 K, 295 K, and 318 K. Rutile had the highest binding capacity for Cr(III) at 295 K with a binding capacity of 11.2 mg/g and brookite had the highest binding capacity for Cr(VI) at 295 K with approximately 15.5 mg/g bound.

Additionally, the thermodynamic studies indicated non-spontaneous reactions for the most part except for chromium (VI) binding to brookite and rutile. Similarly, most reactions were endothermic with the exception of chromium (III) binding to brookite. Furthermore, the sorption of chromium (III) for all three polymorphs occurred through ion-exchange. Chromium (VI) bound to both anatase and rutile via ion-exchange, whereas with rutile it bound via physisorption.

Interference studies were conducted to determine if hard cations and anions effect the binding of the Cr(III) and Cr(VI) ions onto the titanium dioxide polymorph nanomaterials. The

binding of chromium (III) onto anatase appears to have a synergistic effect in which the binding increases with an increase in the cation concentration. Chromium (VI) on the other hand, shows an antagonistic effect in the presence of Cl^-, SO_4^{2-}, and PO_4^{3-} as their respective concentration increases. Nitrate appears to enhance the binding of chromium (VI) onto anatase. The binding of chromium (III) onto brookite in the presence of the individual cations increases as the concentration of the cations increase. Whereas chromium (VI), is unaffected by the presence of anions at low concentrations. However, in the presence of high concentrations for SO_4^{2-} and PO_4^{3-} the binding of chromium(VI) onto brookite is inhibited and a decrease is observed. Lastly, the binding of chromium (III) and chromium (VI) onto rutile appear to follow the same trend as the seen for brookite.

The combined interference study for the binding of chromium (III) onto anatase, brookite, and rutile appears to increase as the concentration of hard cations increases. The binding of chromium(VI) on the other hand, shows a decrease in the binding to the nanomaterials as the concentrations of anions increase.

REFERENCES

[1] Wkh, Zkhuh, et al. *Organic Pollutants in Groundwater : Health Effects*. pp. 5–7.

[2] Iit, Nptel, and Kharagpur Web. *Module 10 : Classification Of Water Pollutants And Effects On Environment Lecture 12 : Classification Of Water Pollutants And Effects On Environment*. pp. 1–7.

[3] Rengaraj, S., et al. "Removal of Chromium from Water and Wastewater by Ion Exchange Resins." *Journal of Hazardous Materials*, vol. 87, no. 1–3, 2001, pp. 273–87, doi:10.1016/S0304-3894(01)00291-6.

[4] Lakherwal, Dimple. "Adsorption of Heavy Metals: A Review." *International Journal of Environmental Research and Development*, vol. 4, no. 1, 2014, pp. 2249–3131, doi:10.1007/s11270-007-9401-5.

[5] EPA. "Chromium in Drinking Water." EPA, Environmental Protection Agency, 24 Apr. 2017, www.epa.gov/dwstandardsregulations/chromium-drinking-water.

[6] A.D.A.M. . "Chromium in Diet." The New York Times, The New York Times, www.nytimes.com/health/guides/nutrition/chromium-in-diet/overview.html.

[7] Cantu, Yvette, et al. "Thermodynamics, Kinetics, and Activation Energy Studies of the Sorption of chromium(III) and chromium(VI) to a Mn3O4 Nanomaterial." *Chemical Engineering Journal*, vol. 254, Elsevier B.V., 2014, pp. 374–83, doi:10.1016/j.cej.2014.05.110.

[8] Barakat, M. A. "New Trends in Removing Heavy Metals from Industrial Wastewater." *Arabian Journal of Chemistry*, vol. 4, no. 4, King Saud University, 2011, pp. 361–77, doi:10.1016/j.arabjc.2010.07.019.

[9] Luther, Steven, et al. "Study of the Thermodynamics of chromium(III) and chromium(VI) Binding to iron(II/III)oxide or Magnetite or Ferrite and magnanese(II) Iron (III) Oxide or Jacobsite or Manganese Ferrite Nanoparticles." *Journal of Colloid and Interface Science*, vol. 400, Elsevier Inc., 2013, pp. 97–103, doi:10.1016/j.jcis.2013.02.036.

[10] Leal, J. H., et al. "Brookite and Anatase Nanomaterial Polymorphs of TiO2 Synthesized from TiCl3." *Inorganic Chemistry Communications*, vol. 84, 2017, pp. 28–32, doi:10.1016/j.inoche.2017.07.014.

[11] B. Grzmil, M. Gleń, B. Kic, K. Lubkowski, Study of the anatase to rutile transformation kinetics of the modified TiO2, Pol. J. Chem. Technol. 15 (2004) 73–80.

[12] W.F. Zhang, Y.L. He, M.S. Zhang, Z. Yin, Q. Chen, Raman scattering study on anatase TiO2 nanocrystals, J. Phys. D. Appl. Phys. 33 (2000) 912–916.

[13] Chowdhury, Papita Saha and Shamik. "Insight Into Adsorption Thermodynamics." *Journal of Hazardous Materials*, vol. 162, 2003, p. 440, doi:10.1007/978-3-642-30391-3.

[14] NPTEL. "Adsorption." *National Programme on Technology Enhanced Learning*, http://nptel.ac.in/courses/122101001/downloads/lec-36.pdf.

[15] Al-Anber, Mohammed. "Thermodynamics Approach in the Adsorption of Heavy Metals." *Intech*, 2011.

[16] Chen, Tao, et al. "Genotoxicity of Titanium Dioxide Nanoparticles." *Journal of Food and Drug Analysis*, vol. 22, no. 1, Elsevier Masson SAS, 2014, pp. 95–104, doi:10.1016/j.jfda.2014.01.008.

[17] Santiago, Ivonne, et al. *Removal of Hexavalent Chromium from Water Using Tailored Zeolites*. 1992, pp. 37–43.

[18] Gasser, M. S., et al. "Batch Kinetics and Thermodynamics of Chromium Ions Removal from Waste Solutions Using Synthetic Adsorbents." *Journal of Hazardous Materials*, vol. 142, no. 1–2, 2007, pp. 118–29, doi:10.1016/j.jhazmat.2006.07.065.

[19] Tel, H., et al. "Adsorption Characteristics and Separation of Cr(III) and Cr(VI) on Hydrous titanium(IV) Oxide." *Journal of Hazardous Materials*, vol. 112, no. 3, 2004, pp. 225–31, doi:10.1016/j.jhazmat.2004.05.025.

[20] Valle, J. P., et al. "Sorption of Cr (III) and Cr (VI) to K 2 Mn 4 O 9 Nanomaterial a Study of the Effect of pH , Time , Temperature and Interferences." *Microchemical Journal*, vol. 133, Elsevier B.V., 2017, pp. 614–21, doi:10.1016/j.microc.2017.04.021.

BIOGRAPHICAL SKETCH

Yvette Cantu was born in Illinois and raised in Roma, TX. She received a Bachelor's of Science in Chemistry with a minor in Biology in 2013 from the University of Texas Pan American in Edinburg, TX. She received a Master's of Science in Chemistry in 2017 from The University of Texas Rio Grande Valley in Edinburg, TX. She is currently teaching science to middle school students.

The author can be reached at the following email address: yvette.cantu02@utrgv.edu